CELL BIOLOGY

Mechanisms of biased agonism by $G\alpha_{i/o}$-biased stapled peptide agonists of the relaxin-3 receptor

Tharindunee Jayakody[1,2,3]†*, Asuka Inoue[4], Srinivasaraghavan Kannan[5], Gaku Nakamura[4], Kouki Kawakami[4], Krishan Mendis[3], Thanh-Binh Nguyen[5]‡, Jianguo Li[5], Deron R. Herr[1]§, Chandra S. Verma[5,6,7], Gavin S. Dawe[1,2,8,9]*

The neuropeptide relaxin-3 is composed of an A chain and a B chain held together by disulfide bonds, and it modulates functions such as anxiety and food intake by binding to and activating its cognate receptor RXFP3, mainly through the B chain. Biased ligands of RXFP3 would help to determine the molecular mechanisms underlying the activation of G proteins and β-arrestins downstream of RXFP3 that lead to such diverse functions. We showed that the i, i+4 stapled relaxin-3 B chains, 14s18 and d(1-7)14s18, were $G\alpha_{i/o}$-biased agonists of RXFP3. These peptides did not induce recruitment of β-arrestin1/2 to RXFP3 by GPCR kinases (GRKs), in contrast to relaxin-3, which enabled the GRK2/3-mediated recruitment of β-arrestin1/2 to RXFP3. Relaxin-3 and the previously reported peptide 4 (an i, i+4 stapled relaxin-3 B chain) did not exhibit biased signaling. The staple linker of peptide 4 and parts of both the A chain and B chain of relaxin-3 interacted with extracellular loop 3 (ECL3) of RXFP3, moving it away from the binding pocket, suggesting that unbiased ligands promote a more open conformation of RXFP3. These findings highlight roles for the A chain and the N-terminal residues of the B chain of relaxin-3 in inducing conformational changes in RXFP3, which will help in designing selective biased ligands with improved therapeutic efficacy.

INTRODUCTION

Relaxin-3 is a neuropeptide of the insulin/insulin-like growth factor/relaxin family. The 51 amino acids of relaxin-3 are organized into an A chain (24 amino acids) and a B chain (27 amino acids) (Fig. 1, A to C). According to the three-dimensional (3D) structure of relaxin-3, the A chain contains two α helices that are separated by a turn. In addition, the A chain is linked to the B chain through two interchain disulfide bonds (Fig. 1C). The B chain contains a central α helix that terminates with a turn (*1*, *2*). Albeit with lower potency, the B chain of relaxin-3 alone can bind to and activate its cognate receptor RXFP3, a class A G protein–coupled receptor (GPCR) (*3*–*8*). Structure-activity relationship studies have revealed that the residues Arg^{8}, Arg^{12}, Ile^{15}, Arg^{16}, Ile^{19}, and Phe^{20} in the central α helix of the relaxin-3 B chain are important for binding to RXFP3 and that these same residues, except for Arg^{12}, are also essential for binding to RXFP4 (*9*, *10*). Moreover, Arg^{26} and Trp^{27} of the C-terminal region of the B chain are essential for the activation of RXFP3 and RXFP4, leading to the conclusion that the first seven amino acid residues of the N-terminal region of the B chain are not essential for binding to or activating the receptor (*11*). Thus, the function of the conserved N-terminal residues is yet to be found. However, the only known function of the A chain is to act as a scaffold to help maintain the α helicity of the B chain (*12*, *13*). Relaxin-3 acts through RXFP3 to modulate important physiological responses, such as the stress response (*14*–*18*); anxiety (*19*–*21*); feeding, metabolism, and weight gain (*22*–*29*); and cognition (*8*, *14*, *30*, *31*). However, the molecular mechanisms and signaling pathways that underlie these functions mediated by the relaxin-3–RXFP3 system are unclear. In addition, as reported from in vitro studies, relaxin-3 binds to and activates RXFP1 (*9*) and RXFP4, although the physiological relevance of these interactions is unclear (*10*, *32*). Therefore, a biased ligand of RXFP3 that could induce ligand-specific and distinct conformations of the receptor, resulting in different intrinsic activities, potencies, or both for different signaling pathways by interacting with distinct downstream effectors, would be a useful tool in delineating pathways and molecular mechanisms leading to the diverse functions of this system (*33*, *34*).

Previously, in an attempt to develop a single-chain RXFP3 agonist, our group and others provided evidence that hydrocarbon stapling, in which two (*S*)2-(4′-pentenyl)alanine nonnatural amino acids are substituted for the residues at the i and i+4 positions of the B chain, followed by a ring-closing metathesis (RCM) reaction, formed cross-links (staples) that successfully produced helical, protease-resistant, single-chain analogs of the relaxin-3 B chain, which would otherwise appear as random coils. These stapled B chains are biologically active because of the α helicity that is essential for binding to and activating RXFP3 (*20*, *35*–*37*). As observed previously with ligands of GPCRs, such as the dopamine and serotonin receptor subtypes (D2 receptors and 5-HT_{2c} receptors), even minor structural changes to the ligand may induce ligand bias at GPCRs (*38*). Such evidence led us to investigate the functional selectivity of the 14s18 stapled peptide, in which the relaxin-3 B chain is stapled at two mutated sites, Phe^{14}→Ser (F14S) and Val^{18}→Ser (V18S) (Fig. 1, A, B, and D)

[1]Department of Pharmacology, Yong Loo Lin School of Medicine, National University of Singapore, Singapore. [2]Neurobiology Programme, Life Sciences Institute, National University of Singapore, Singapore. [3]Department of Chemistry, University of Colombo, P.O. Box 1490, Colombo 00300, Sri Lanka. [4]Graduate School of Pharmaceutical Sciences, Tohoku University, Sendai 980-8578, Japan. [5]Bioinformatics Institute, A*STAR, 30 Biopolis Street, #07-01 Matrix, Singapore 138671. [6]Department of Biological Sciences, National University of Singapore, 6 Science Drive 4, Singapore 117558. [7]School of Biological Sciences, Nanyang Technological University, 60 Nanyang Dr., Singapore 637551. [8]Healthy Longevity Translational Research Programme, Yong Loo Lin School of Medicine, National University of Singapore, Singapore. [9]Precision Medicine Translational Research Programme, Yong Loo Lin School of Medicine, National University of Singapore, Singapore.
*Corresponding author. Email: tharindunee@chem.cmb.ac.lk (T.J.); phcdgs@nus.edu.sg (G.S.D.)
†Present address: Department of Chemistry, University of Colombo, P.O. Box 1490, Colombo 00300, Sri Lanka.
‡Present address: School of Chemistry and Molecular Biosciences, University of Queensland, Chemistry Bld, 68 Cooper Rd, Brisbane City, QLD 4067, Australia.
§Present address: Translational Neuroscience Initiative, Sanford Burnham Prebys Medical Discovery Institute, La Jolla, CA 92037, USA.

(*36*, *37*). In addition, because there are no previous reports of the importance of the first seven amino acids of the B chain to the binding or activation of RXFP3, we designed the d(1-7)14s18 form of the B chain, which is truncated (missing residues 1 to 7) and hydrocarbon-stapled at F14S and V18S to validate the signaling profiles of the 14-18 stapled B chains (Fig. 1, A, B, and E). To assess the effect of the F14S and V18S mutations, two control peptides with identical mutations [double mutant (DM)] were designed. In the B chain DM, the entire B chain was included with the F14S and V18S mutations, whereas in the d(1-7)B chain DM, the first seven residues of the B chain were eliminated. Furthermore, to determine whether changes to the stapling position resulted in similar or variable signaling profiles, we determined the functional selectivity of peptide 4, which is hydrocarbon-stapled at the mutated sites Glu^{13}→Ser (E13S) and Ala^{17}→Ser (A17S) of the B chain with a similar deletion of the N-terminal region of the B chain as was made for d(1-7)14s18 (Fig. 1, A, B, and F) (*35*). Here, we used quantitative signaling assays to generate concentration-response curves and the operational model of agonism proposed by Black and Leff to determine transduction ratio values (τ/K_A) for each signaling pathway. This parameter includes both intrinsic efficacy (τ) and affinity (K_A) for each of the ligand-receptor-effector complexes, considering the importance of allosterism of the three molecules in the activation of a signaling pathway. Using the derived transduction ratio values, the biased factor for each pathway is then calculated. (*39*). In addition, computational modeling of the ligand-RXFP3 complexes and in vitro signaling assays were used to determine the molecular mechanisms underlying the functional selectivity of these peptides.

RESULTS

H3 relaxin and stapled peptide analogs activate $G\alpha_{i/o}$

We used the NanoBiT–G protein dissociation assay with five representative G protein sensors ($G\alpha_{i1}$, $G\alpha_o$, $G\alpha_q$, $G\alpha_s$, and $G\alpha_{13}$) to measure and validate previously published data on the G protein–coupling characteristics of RXFP3 upon stimulation with human relaxin-3 (H3 relaxin) (*40*) and to determine whether 14s18 promoted a similar pattern (Fig. 2, A to E). As reported previously, H3 relaxin stimulated RXFP3 to primarily couple to $G\alpha_{i/o}$ (Fig. 2, B and C). Similarly, RXFP3 stimulation by 14s18 also induced $G\alpha_{i/o}$ coupling (Fig. 2, B and C). Furthermore, both H3 relaxin and 14s18 induced relatively weaker coupling to $G\alpha_q$ and $G\alpha_{13}$ (Fig. 2, D and E).

Next, we used an enzyme-linked immunosorbent assay (ELISA)–based inhibition of forskolin-induced cyclic adenosine monophosphate (cAMP) assay to generate concentration-response curves for the activation of the $G\alpha_{i/o}$ pathway by H3 relaxin and the H3 relaxin B-chain analogs in human embryonic kidney (HEK) 293T cells stably expressing RXFP3 (HEK-RXFP3 cells). Of the six ligands tested, H3 relaxin displayed the highest potency [a -$\log EC_{50}$ (pEC_{50}) value of 9.43 ± 0.08] for activation of the $G\alpha_{i/o}$ pathway in HEK-RXFP3 cells. For the same pathway, the stapled peptides displayed lower potency values with peptide 4 (pEC_{50} = 8.31 ± 0.18) (*35*) and 14s18 (pEC_{50} = 7.90 ± 0.24) displaying intermediate potencies, and d(1-7)14s18 displaying the lowest potency (pEC_{50} = 7.71 ± 0.42). H3 relaxin and the stapled peptides showed the same pattern for efficacy (E_{max}), with H3 relaxin displaying the highest E_{max} value of 88.45 ± 2. Peptide 4 (E_{max} = 75.64 ± 3) was the most efficacious of the stapled peptides tested, which was followed by 14s18 (E_{max} = 60.98 ± 5) and d(1-7)14s18 (E_{max} = 50.16 ± 8) (Fig. 2F and Table 1). However, the unstapled analogs of the stapled peptides, B chain DM and d(1-7)B chain DM, were markedly less potent, with pEC_{50} values <7, but they displayed higher E_{max} values [the E_{max} of the B chain DM was 113.6 ± 1, whereas that of the d(1-7)B chain DM was 83.73 ± 5 at concentrations >1 μM (Fig. 2G and Table 1)]. We generated concentration-response data for H3 relaxin, 14s18, d(1-7)14s18 (Fig. 2H), and the B chain DM and d(1-7)B chain DM peptides (Fig. 2I) for wild-type (WT) HEK293T cells that do not express RXFP3. The results revealed that none of the peptides showed notable

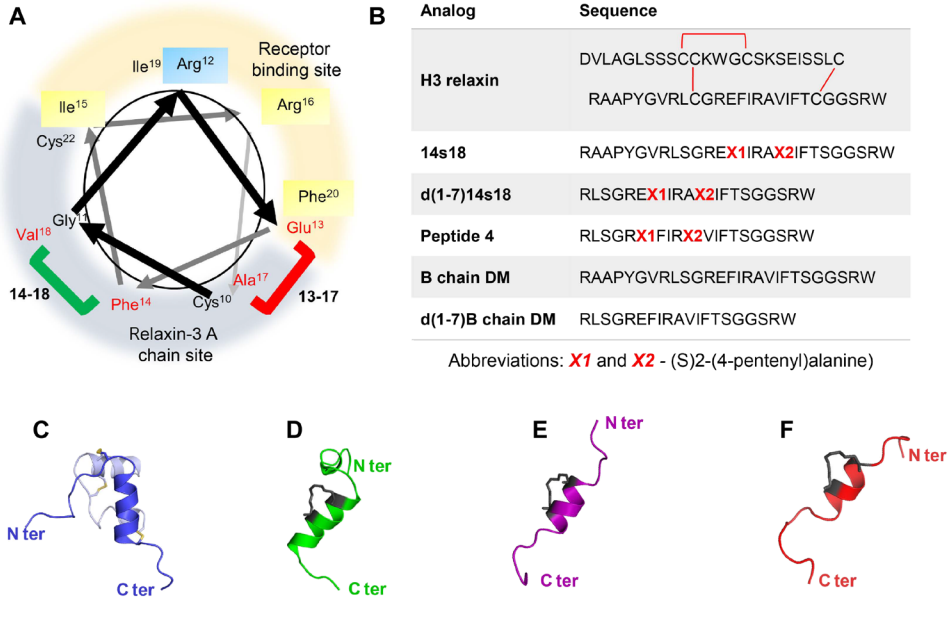

Fig. 1. Sequences and structures of the peptides used in this study. (**A**) Helical wheel diagram that depicts the α helix of the human relaxin-3 (H3 relaxin) B chain from the N terminus to the C terminus. The side of the α helix that interacts with RXFP3 is highlighted in yellow, and the side that interacts with the A chain is highlighted in gray. The amino acids are indicated with their residue numbers. The residues mutated during stapling are indicated in red, residues involved in binding to RXFP3 and RXFP4 are highlighted in yellow, and the residue involved in RXFP3 activation is highlighted in blue. The position of the staple of the stapled B chains is indicated in green and red square brackets. (**B**) Sequences of the peptides used in this study. (**C**) The 3D structure of H3 relaxin (blue). (**D**) The 3D structure of 14s18 (green). (**E**) The 3D structure of d(1-7)14s18 (purple). (**F**) The 3D structure of peptide 4 (red). The N-terminal (N ter) and C-terminal (C ter) ends of the peptides are labeled accordingly (*35*–*37*). The structures of the stapled peptides 14s18, d(1-7)14s18, and peptide 4 were constructed from the NMR solution structure of relaxin-3 (PDB: 2FHW), each with staples (in gray) bridging different positions (14 to 18 and 13 to 17) and modeled. Structural models of the bound state of relaxin-3 on RXFP3 were generated with the program Modeller 9v18.

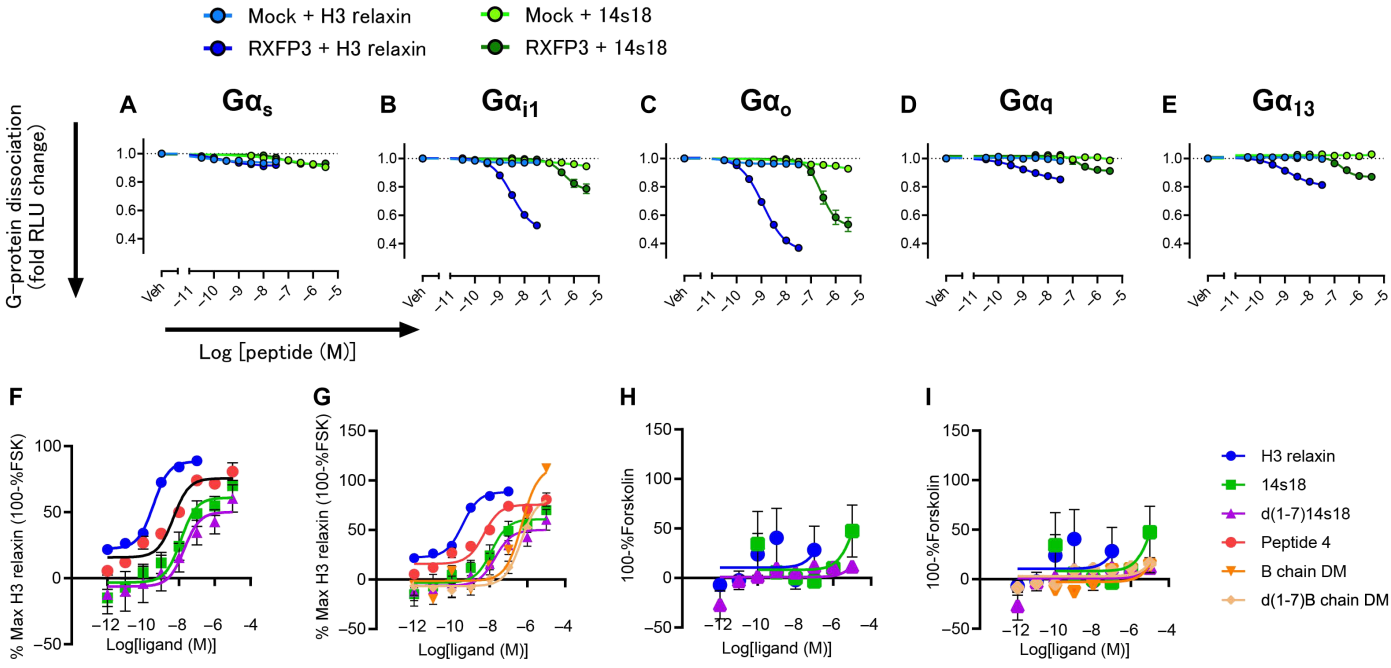

Fig. 2. G protein profile of RXFP3 and Gα$_{i/o}$ activation by H3 relaxin and analogs. (**A** to **E**) G protein activation profile of RXFP3 by vehicle (Veh), H3 relaxin (10 pM to 100 nM), and 14s18 (10 pM to 10 μM). (**F** and **G**) Concentration-response curves for Gα$_{i/o}$ activation in (F) (test peptides) and (G) (test and control peptides) in HEK-RXFP3 cells by H3 relaxin (1 pM to 100 nM), 14s18 (1 pM to 10 μM), d(1-7)14s18 (1 pM to 10 μM), B chain DM (1 pM to 10 μM), d(1-7)B chain DM (1 pM to 10 μM), and peptide 4 (1 pM to 10 μM). (**H** and **I**) Concentration-response curves for Gα$_{i/o}$ activation (H, test peptides) and (I, test and control peptides) in WT HEK293T cells by H3 relaxin (1 pM to 100 nM), 14s18 (1 pM to 10 μM), d(1-7)14s18 (1 pM to 10 μM), B chain DM (1 pM to 10 μM), and d(1-7)B chain DM (1 pM to 10 μM) cells. Data in (A) to (E) were obtained using a NanoBiT–G protein dissociation assay and are from three independent experiments. Data in (F) to (I) were obtained using an inhibition of forskolin (FSK)–induced cAMP assay. The cAMP concentration is represented as a percentage of the maximum response to H3 relaxin derived from 100 − % forskolin-induced response in (F) and (G) and 100 − % forskolin-induced response in (H) and (I). Data are means ± SEM of three or four independent experiments each performed in triplicate. Curves were fitted using a four-parameter Hill equation: Y = Bottom + (Top − Bottom)/(1 + 10^(logEC_{50} − X)).

concentration-dependent activation of the Gα$_{i/o}$ pathway in these cells, confirming that activation of the Gα$_{i/o}$ pathway by H3 relaxin and its stapled peptide analogs in HEK-RXFP3 cells was RXFP3-specific.

H3 relaxin and peptide 4, but not 14s18 and d(1-7)14s18, stimulate β-arrestin recruitment to RXFP3

We next established a NanoBiT enzyme complementation assay to generate concentration-response curves for the recruitment of β-arrestin1 and β-arrestin2 to RXFP3. The initial optimization of the transfection conditions, whereby cells were treated with 10 nM H3 relaxin, revealed that higher and more stable luminescence could be obtained when the cells were cotransfected with 100 ng of pCAGGS-LgBiT-ARRB1 or pCAGGS-LgBiT-ARRB2 together with 200 ng of pCAGGS-RXFP3-SmBiT and then assayed with the substrate coelenterazine h (Fig. 3, A to C). Thus, we used these conditions to generate concentration-response curves.

Table 1. Potencies (pEC_{50} values) and relative efficacies (E_{max} values) for Gα$_{i/o}$ activation and β-arrestin1 and β-arrestin2 recruitment by peptide-activated RXFP3. Data are means ± SEM of three or four independent experiments, each performed in triplicate or duplicate. ND, not determined (because of the absence of a concentration response).

Ligand	Inhibition of FSK-induced cAMP (Gα$_{i/o}$ activation)		β-Arrestin1 recruitment		β-Arrestin2 recruitment	
	pEC_{50}	E_{max}	pEC_{50}	E_{max}	pEC_{50}	E_{max}
H3 relaxin	9.43 ± 0.08	88.45 ± 2	8.37 ± 0.12	102.4 ± 5	8.15 ± 0.12	94.84 ± 3
14s18	7.90 ± 0.24	60.98 ± 5	ND	ND	ND	ND
d(1-7)14s18	7.71 ± 0.42	50.16 ± 8	6.42 ± 1.99	2.53 ± 6	ND	ND
Peptide 4	8.31 ± 0.18	75.64 ± 3	7.60 ± 0.23	81.4 ± 2	7.43 ± 0.14	85.48 ± 1
B chain DM	6.29 ± 0.17	113.6 ± 1	<6	ND	<6	ND
d(1-7)B chain DM	6.34 ± 0.10	83.73 ± 5	<6	ND	<6	ND

Similarly to the results from our $G\alpha_{i/o}$ pathway activation studies, H3 relaxin displayed the highest potency for the recruitment of β-arrestin1 ($pEC_{50} = 8.37 \pm 0.12$) (Fig. 3, D and E, and Table 1) and β-arrestin2 ($pEC_{50} = 8.15 \pm 0.12$) (Fig. 3, F and G, and Table 1) to RXFP3. Both the stapled peptides 14s18 and d(1-7)14s18 and the respective unstapled B chains displayed little or no recruitment of β-arrestin1 (Fig. 3E and Table 1) or β-arrestin2 (Fig. 3G and Table 1) up to concentrations of 1 μM. In contrast to the 14-18 stapled B chains, the 13-17 stapled B chain (peptide 4) (*35*) displayed β-arrestin1 recruitment to RXFP3 with a potency of 7.60 ± 0.23 (Fig. 3, D and E, and Table 1) and an efficacy (E_{max}) of 81.4 ± 2, as well as β-arrestin2 recruitment to RXFP3 with a potency of 7.43 ± 0.14 and an E_{max} of 85.48 ± 1 (Fig. 3, F and G, and Table 1).

14s18 and d(1-7)14s18 display bias in activating the $G\alpha_{i/o}$ pathway as compared with recruiting β-arrestin1/2

On the basis of the concentration-response curves for the activation of $G\alpha_{i/o}$ signaling and the recruitment of β-arrestin1 and β-arrestin2 (β-arrestin1/2), we chose H3 relaxin as the reference ligand for bias factor calculations. We analyzed the concentration responses of the stapled peptides for each pathway by the operational model to determine transduction ratio values indicated by $\log(\tau/K_A)$ (also referred to as log*R*). H3 relaxin displayed similar transduction ratio values for the three pathways tested (9.19 ± 0.16 for $G\alpha_{i/o}$ activation, 8.08 ± 0.06 for β-arrestin1 recruitment, and 7.92 ± 0.04 for β-arrestin2 recruitment; Table 2). Transduction ratios for peptide 4 were lower than those of H3 relaxin for $G\alpha_{i/o}$ activation (8.45 ± 0.52), β-arrestin1 recruitment (7.32 ± 0.19), and β-arrestin2 recruitment (7.30 ± 0.14). Both 14s18 and d(1-7)14s18 displayed lower $\log(\tau/K_A)$ values for $G\alpha_{i/o}$ activation (8.02 ± 0.01 and 7.37 ± 0.09, respectively) relative to those of peptide 4 and H3 relaxin, but no $\log(\tau/K_A)$ values could be generated for either peptide for β-arrestin1 and β-arrestin2 pathway recruitment because of the lack of a concentration response (Table 2).

We then performed within-pathway comparisons using H3 relaxin as a reference ligand to calculate $\Delta\log(\tau/K_A)$ or $\Delta\log R$ values and determined relative effectiveness for $G\alpha_{i/o}$ pathway activation and β-arrestin1 and β-arrestin2 recruitment (Table 2). Statistical analysis of the $\Delta\log(\tau/K_A)$ values was performed by analysis of variance (ANOVA) for $G\alpha_{i/o}$ activation and by one-sample *t* test for β-arrestin1 and β-arrestin2 recruitment. These data showed that the relative effectiveness of peptide 4 at $G\alpha_{i/o}$ activation (0.18), β-arrestin1 recruitment (0.17), and β-arrestin2 recruitment (0.24) was not statistically different from that of H3 relaxin (1 for all three pathways). We observed significant reductions in the relative effectiveness of $G\alpha_{i/o}$ pathway activation compared with that of H3 relaxin for 14s18 (0.07) and d(1-7)14s18 (0.02). However, $\Delta\log(\tau/K_A)$ could not be calculated for the 14-18 stapled peptides for β-arrestin1 and β-arrestin2 recruitment because of the absence of transduction coefficient values (Table 2).

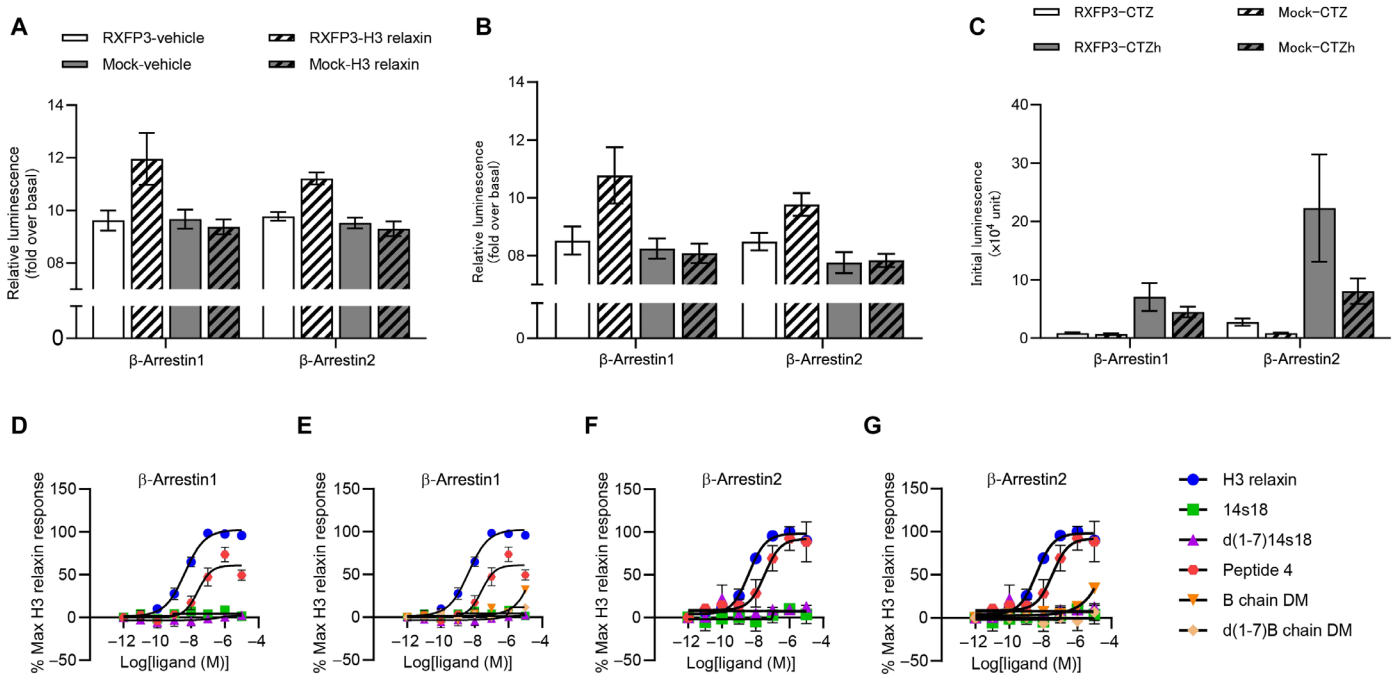

Fig. 3. NanoBiT β-arrestin recruitment assay to detect β-arrestin1 and β-arrestin2 recruitment to RXFP3 after activation by H3 relaxin and its analogs in HEK293 cells. (**A** to **C**) When establishing the assay, luminescence was detected in the presence of (A) 10 μM coelenterazine (CTZ) and (B) 10 μM coelenterazine h (CTZh) after treatment with 10 nM H3 relaxin or vehicle. (C) Initial luminescent counts with 10 μM coelenterazine and 10 μM coelenterazine h. Data are means ± SEM of three or four independent experiments each performed in duplicate or triplicate. (**D** and **E**) Test peptides (D) and test and control peptides (E). Concentration-response curves for β-arrestin1 recruitment to RXFP3 activated by H3 relaxin, 14s18, d(1-7)14s18, B chain DM, d(1-7)B chain DM, and peptide 4 (1 pM to 10 μM). (**F** and **G**) Test peptides (F) and test and control peptides (G). β-Arrestin2 recruitment to RXFP3 activated by H3 relaxin, 14s18, d(1-7)14s18, B chain DM, d(1-7)B chain DM, and peptide 4 (1 pM to 10 μM). β-Arrestin1 and β-arrestin2 recruitment are represented as the percentage of the maximal H3 relaxin response of the area under the curve (AUC) of ligand:basal luminescence ratios versus time. Data are means ± SEM of three to eight independent experiments each performed in triplicate or in duplicate. Curves were fitted using a four-parameter Hill equation: $Y = \text{Bottom} + (\text{Top} - \text{Bottom})/(1 + 10\text{^}(\log_{EC50} - X))$.

Table 2. Transduction ratios [log(τ/K_A)] of H3 relaxin, 14s18, d(1-7)14s18, and peptide 4 for $G\alpha_{i/o}$ activation and β-arrestin1 and β-arrestin2 recruitment by activated RXFP3 in HEK-RXFP3 cells. Data are means ± SEM of three or four independent experiments, each performed in triplicate or duplicate. $\Delta\log(\tau/K_A)$ ratios were analyzed by ANOVA, followed by Dunnett's post hoc test comparing each stapled peptide with H3 relaxin for $G\alpha_{i/o}$ activation and by one-sample *t* test comparing peptide 4 with H3 relaxin for β-arrestin1 and β-arrestin2 recruitment to determine the significance of the relative effectiveness for each pathway. $^{**}P < 0.001$.

Ligand	Inhibition of FSK-induced cAMP ($G\alpha_{i/o}$ activation)			β-Arrestin1			β-Arrestin2		
	Log*R*	ΔLog*R*	RE	Log*R*	ΔLog*R*	RE	Log*R*	ΔLog*R*	RE
H3 relaxin	9.19 ± 0.16	0.00 ± 0.11	1.00	8.08 ± 0.06	0.00 ± 0.10	1.00	7.92 ± 0.04	0.00 ± 0.06	1.00
14s18	8.02 ± 0.01	−1.17 ± 0.08	0.07**	ND	ND	ND	ND	ND	ND
d(1-7)14s18	7.37 ± 0.09	−1.82 ± 0.12	0.02**	ND	ND	ND	ND	ND	ND
Peptide 4	8.45 ± 0.52	−0.74 ± 0.31	0.18	7.32 ± 0.19	−0.76 ± 0.20	0.17	7.30 ± 0.14	−0.62 ± 0.15	0.24

Next, we performed between-pathway comparisons to calculate the bias factor (BF) in the form of ΔΔlog*R* values and compared Δlog*R* values for $G\alpha_{i/o}$ pathway activation and β-arrestin1 and β-arrestin2 recruitment pathways by one-way ANOVA (Table 3). These bias factors showed that peptide 4 activated the $G\alpha_{i/o}$ pathway and stimulated β-arrestin1 recruitment (ΔΔlog*R* value of 0.02 ± 0.37) and β-arrestin2 recruitment (ΔΔlog*R* value of −0.12 ± 0.34) with no significant bias toward either pathway. Both 14s18 and d(1-7)14s18 only activated the $G\alpha_{i/o}$ pathway and did not stimulate β-arrestin recruitment, suggesting that they were biased toward $G\alpha_{i/o}$ pathway activation (Table 3).

β-Arrestin recruitment to RXFP3 is mediated by GRK2 and GRK3 in response to H3 relaxin but not in response to biased peptides

We used a NanoBiT enzyme complementation assay as described earlier to determine the specific GPCR kinase (GRK) subtype (from GRK2, GRK3, GRK5, and GRK6) that phosphorylated RXFP3 to facilitate the recruitment of β-arrestin1 and β-arrestin2 in response to H3 relaxin and 14s18 (Fig. 4). In HEK293 cells that expressed RXFP3 but not these GRK subtypes, neither H3 relaxin nor 14s18 resulted in a concentration-response curve for the recruitment of β-arrestin1 (Fig. 4A) or β-arrestin2 (Fig. 4F). However, in HEK293 cells that expressed RXFP3 and GRK2, H3 relaxin stimulated β-arrestin1 recruitment (pEC_{50} = 8.14 ± 0.10) (Fig. 4B) and β-arrestin2 recruitment (pEC_{50} = 8.69 ± 0.12) (Fig. 4G). Similarly, in HEK293 cells that expressed RXFP3 and GRK3, H3 relaxin stimulated β-arrestin1 recruitment (pEC_{50} = 8.07 ± 0.07) (Fig. 4C) and β-arrestin2 recruitment (pEC_{50} = 8.74 ± 0.17) (Fig. 4H). Treating HEK293 cells expressing RXFP3 and either GRK2 or GRK3 with 14s18 did not induce β-arrestin1 or β-arrestin2 recruitment to RXFP3 (Fig. 4, B, C, G, and H). Moreover, treating HEK293 cells expressing RXFP3 and GRK5 or GRK6 with either H3 relaxin or 14s18 did not elicit concentration-dependent recruitment of β-arrestin1 (Fig. 4, D and E) or β-arrestin2 (Fig. 4, I and J).

14s18 and d(1-7)14s18 display reduced potencies for ERK1/2 activation and SRE reporter gene expression

We used a homogeneous time-resolved fluorescence (HTRF) extracellular signal–regulated kinase 1/2 (ERK1/2) activation assay and a luciferase serum response element (SRE) reporter gene activation assay to detect changes in the signaling pathways downstream of the $G\alpha_{i/o}$-biased stapled peptides. During the optimization of the ERK1/2 assay, we treated HEK-RXFP3 cells with H3 relaxin for 8 min and then incubated cells in lysis buffer for 1 or 2 hours to facilitate cell lysis. The results indicated that a quantifiable concentration response was obtained after 2 hours of cell lysis (fig. S1). Therefore, we used these optimal conditions in the subsequent experiments to generate concentration-response curves. H3 relaxin activated ERK1/2 (pEC_{50} = 9.46 ± 0.16), whereas 14s18 and d(1-7)14s18 did not show concentration-dependent responses (Fig. 5A and Table 4).

Table 3. $\Delta\Delta\log(\tau/K_A)$ ratios and BF values for stapled B chains of H3 relaxin. Data are means ± SEM of three or four independent experiments, each performed in triplicate or duplicate. $\Delta\log(\tau/K_A)$ ratios were analyzed by ANOVA, followed by Bonferroni post hoc test comparing the $\Delta\log(\tau/K_A)$ value for one pathway with that of the other (cAMP with β-arrestin1 or β-arrestin2), where no significant difference was observed between pathways for peptide 4.

Ligand	cAMP-β arrestin1		cAMP-β arrestin2	
	ΔΔLog*R*	BF	ΔΔLog*R*	BF
H3 relaxin	0.00 ± 0.15	1.00	0.00 ± 0.13	1.00
14s18	ND	ND	ND	ND
d(1-7)14s18	ND	ND	ND	ND
Peptide 4	0.02 ± 0.37	1.05	−0.12 ± 0.34	0.76

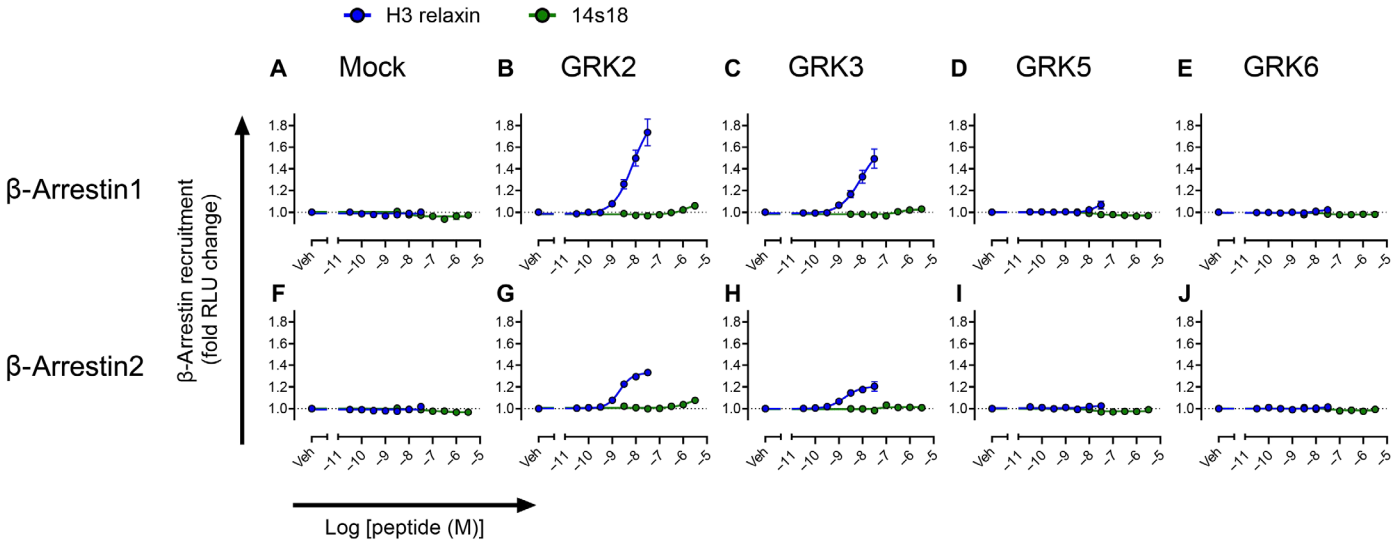

Fig. 4. β-Arrestin recruitment to RXFP3 in the presence of GRK subtypes by H3 relaxin and 14s18. (**A** to **J**) β-Arrestin activity and GRK subtype bias detected by NanoBiT β-arrestin recruitment assay in HEK293 cells in response to vehicle (Veh), H3 relaxin (1 pM to 100 nM), and 14s18 (1 pM to 10 μM). Recruitment of β-arrestin1 (A to E) and β-arrestin2 (F to J) was determined in HEK293 cells expressing RXFP3 and transfected with (A and F) control expression plasmid, (B and G) GRK2 expression vector, (C and H) GRK3 expression vector, (D and I) GRK5 expression vector, or (E and J) GRK6 expression vector. Data are means ± SEM of three independent experiments. Curves were fitted using a four-parameter Hill equation: $Y = \text{Bottom} + (\text{Top} - \text{Bottom})/(1 + 10\text{^}(\log_{EC50} - X))$.

Optimization of luciferase SRE reporter gene activation assays with HEK-RXFP3 cells treated with 100 nM H3 relaxin revealed that the luciferase activity was significantly increased after treatment for 4 hours with H3 relaxin (fig. S2A), and transfection of the cells with 100 ng of the pGL4.33-SRE-luciferase vector was optimal, with less variability within treatments generating a concentration-response curve with higher potency (fig. S2, B to D). These conditions were used in our subsequent assays in generating concentration-response curves. In the luciferase SRE reporter gene activation assay, H3 relaxin displayed a pEC_{50} value of 8.81 ± 0.29 (Fig. 5B and Table 4). Both of the stapled peptide ligands activated SRE reporter gene activation with reduced potencies ($pEC_{50} < 6$, Fig. 5B and Table 4). In HEK293T cells, neither RXFP3 agonist stimulated any concentration-dependent response for SRE reporter gene activation (Fig. 5C). Similarly, ERK1/2 activation is not detected in HEK293T cells treated with H3 relaxin (*36*). This confirms that SRE reporter gene activation in HEK-RXFP3 cells is mediated only by RXFP3 with no activation of related receptors. As reported previously, ERK1/2 activation is partially inhibited by inhibition of receptor endocytosis but not by inhibition of β-arrestin1 recruitment (*40*, *41*). Thus, this inhibition of ERK1/2 activation and subsequent SRE reporter gene activation may be due to the lack of β-arrestin2 recruitment.

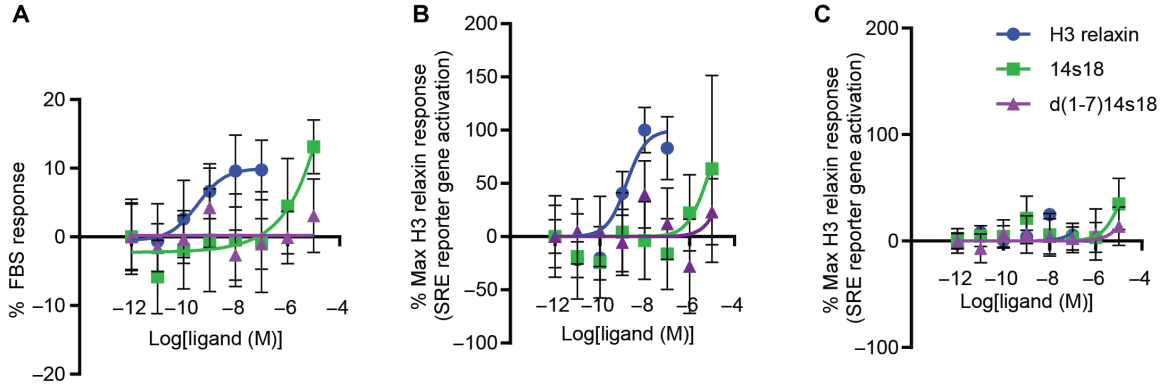

Fig. 5. ERK1/2 and SRE reporter gene activation by H3 relaxin and biased agonists. (**A** to **C**) Concentration-response curves for (A) ERK1/2 activation in HEK-RXFP3 cells, (B) SRE reporter gene activation in HEK-RXFP3 cells, and (C) SRE reporter gene activation in HEK293T cells in response to H3 relaxin (1 pM to 100 nM), 14s18 (1 pM to 10 μM), and d(1-7)14s18 (1 pM to 10 μM). ERK1/2 activation is represented as a percentage of the response to 10% FBS. Data are means ± SEM of three independent experiments. SRE reporter gene activation is represented as a percentage of the maximal response to H3 relaxin. Data are means ± SEM of three independent experiments with HEK-RXFP3 cells and two independent experiments with HEK293T cells, each performed with three to six replicates. Curves were fitted using a four-parameter Hill equation: $Y = \text{Bottom} + (\text{Top} - \text{Bottom})/(1 + 10\text{^}(\log_{EC50} - X))$.

Table 4. Potencies (pEC_{50} values) and relative efficacies (E_{max} values) for H3 relaxin, 14s18, and d(1-7)14s18 for ERK1/2 activation and SRE reporter gene activation by activated RXFP3 in HEK-RXFP3 cells. Data are means ± SEM of three independent experiments, each performed in triplicate.

Ligand	ERK1/2 activation		SRE reporter gene activation	
	pEC_{50}	E_{max}	pEC_{50}	E_{max}
H3 relaxin	9.46 ± 0.16	9.7 ± 0.47	8.81 ± 0.29	74.86 ± 5
14s18	<5	ND	<6	ND
d(1-7)14s18	ND	ND	<6	ND

Only the unbiased ligands peptide 4 and H3 relaxin induce conformational changes in ECL3, TM6, and TM7 of RXFP3 in silico

Using the crystal structure of the angiotensin II receptor in an activated state [Protein Data Bank (PDB): 5XJM and PDB: 6DO1] as a template, a homology model of RXFP3 was constructed and used for modeling complexes of RXFP3 and H3 relaxin and stapled peptides (Fig. 6). In silico docking calculations suggested that the stapled peptides peptide 4, 14s18, and d(1-7)14s18 share modes of binding to RXFP3 that overlap with the binding modes of H3 relaxin, especially the B chain of H3 relaxin. Moreover, the three stapled peptides retain the central helix of the B chain of H3 relaxin, and all three peptides use the positively charged residues Arg^{26}, Arg^{16}, and Arg^{12} for binding to RXFP3. The C-terminal tails of the stapled peptides and of the H3 relaxin B chain are disordered in solution, and the tails remain largely unstructured upon binding (Fig. 6). Trp^{27} of the stapled peptides and the B chain of H3 relaxin are buried deeply into the receptor pocket and engaged in an edge-to-face stacking interaction with $Trp138^{2.60}$ of the receptor. In the case of d(1-7)14s18 and 14s18, the backbone carbonyl of Trp^{27} interacts with the side chains of $Ser159^{3.29}$ and $Thr162^{3.32}$ of the receptor, and in the case of peptide 4, the backbone carbonyl of Trp^{27} interacts with the side chains of $Lys271^{5.42}$, $Tyr267^{5.38}$, and $Ser232^{4.60}$ of the receptor. In the case of d(1-7)14s18 and 14s18, the side chain of Ser^{25} interacts with the side chains of $Asn342^{6.51}$ and $Lys271^{5.42}$ of the receptor, the backbone of Gly^{23} interacts with the side chain of $Tyr363^{ECL3}$ of the receptor, and the backbone of Thr^{21} interacts with the side chain of $Lys353^{6.62}$ of the receptor. In the case of peptide 4, the backbone of Gly^{24} interacts with the side chain of $Ser349^{6.58}$ of the receptor, and the backbone of Cys^{22} interacts with the side chain of $His268^{5.39}$ of the receptor. In addition, the binding of peptides to the receptor is further driven by strong charge-charge interactions: Arg^{26}, Arg^{16}, and Arg^{12} of either peptide are involved in salt-bridge/charge-charge interactions with $Glu141^{ECL1}$, Glu^{77}, and $Asp145^{ECL1}$ of the receptor. In addition, Arg^{8} of peptide 4 forms a salt bridge with $Glu244^{ECL2}$ of the receptor (fig. S3).

During the molecular dynamics (MD) simulations, the binding poses of peptide 4 and 14s18 observed in the docking calculations remained stable with a root mean square deviation (RMSD) of ~3 Å against the respective docked poses. The stacking interactions between Trp^{27} of the peptides and $Trp138^{2.60}$ of RXFP3 were well-preserved during the MD simulations. However, the H-bond interactions observed in the docked poses were quite transient in nature and were observed for less than 50% of the simulation time. In contrast, the salt bridge interactions involving charged residues from the receptor and the peptides were well-preserved during the simulations. In the case of the 14s18 peptide, the staple linker was exposed to solvent and did not interact with any of the residues from RXFP3. Extracellular loop 3 (ECL3), between transmembrane 6 (TM6) and TM7, adopted a closed conformation (Figs. 6 and 7). In

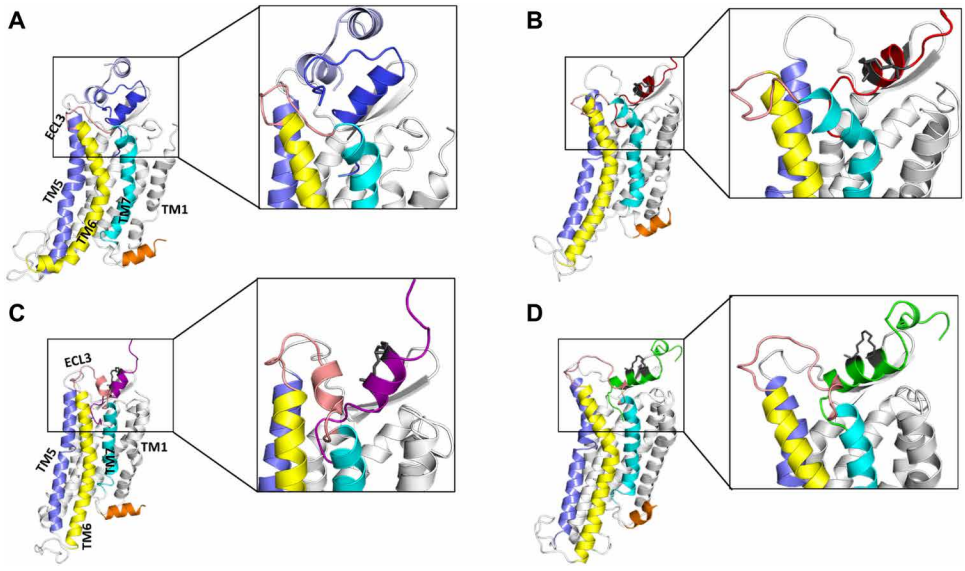

Fig. 6. Structures of complexes formed between RXFP3 and H3 relaxin or stapled peptides. (**A** to **D**) MD snapshots of the structures of (A) RXFP3–H3 relaxin (the A chain and B chain are highlighted in light and dark shades of blue), (B) RXFP3–peptide 4, (C) RXFP3–d(1-7)14s18, and (D) RXFP3-14s18. Both RXFP3 and the stapled peptides are shown as cartoons with the transmembrane helices (TM1, gray; TM5, blue; TM6, yellow; TM7, cyan) and extracellular loop 3 (ECL3, salmon) of RXFP3 and the bound stapled peptides/H3 relaxin highlighted in different colors. In (B) to (D), the staple linker is highlighted in dark gray.

contrast, the staple linker in the case of peptide 4 faced ECL3 between TM6 and TM7 and pushed ECL3 outward (of the pocket) (Fig. 7), thus stabilizing ECL3 together with the extracellular regions of TM6 and TM7 in a more open conformation (fig. S4). The movements of ECL3 and the extracellular regions of TM6 and TM7 induced by peptide 4 resulted in movements of the intracellular regions of TM6 and TM7 helices, which were absent when bound by 14s18 (Fig. 8). The TM6 and TM7 helices adopted more open conformations at the intracellular side in the case of peptide 4 as compared with 14s18 (Fig. 6). H3 relaxin produced a similar opening of the pocket, pushing ECL3 outward (Figs. 6 and 7) and opening the conformation of TM6 and TM7 at the intracellular side (Fig. 6). In the case of H3 relaxin, the interaction with ECL3 was mediated by the A chain in combination with the N terminus of the B chain. The disulfide bridge between Cys^{11} (A chain) and Cys^{10} (B chain) prevented the flexibility of the N-terminal of the B chain, whereas the backbone interactions between Cys^{11} (A chain) and Arg^{8} (B chain) and between Cys^{15} (A chain) and Val^{7}/Gly^{6} (B chain) positioned the N-terminal residues Arg^{1}, Ala^{2}, Ala^{3}, and Tyr^{5} of the B chain so that they could interact with ECL3. In addition, the interactions between Ser^{16} (A chain) and $Pro358^{ECL3}$ and between Lys^{17} (A chain) and $Val357^{ECL3}$/$Asn355^{ECL3}$ further induced opening of the conformation of ECL3 (fig. S5). These interactions between H3 relaxin and peptide 4 with the ECL3 of RXFP3 resulted in reducing the flexibility of ECL3 and the extracellular regions of TM6 and TM7 (Fig. 8, A and B); in contrast, the lack of interactions between ECL3 with 14s18 enhanced the flexibilities of ECL3 and the extracellular regions of TM6 and TM7 (Fig. 8C). Similarly, the flexibilities of the intracellular regions of TM6 and TM7 were reduced when H3 relaxin or peptide 4 was bound compared with when 14s18 was bound.

DISCUSSION

In this study, we demonstrated that peptide ligands synthesized by hydrocarbon stapling of the relaxin-3 B chain at F14S and V18S stimulated $G\alpha_{i/o}$-biased signaling by RXFP3. This conclusion is consistent with previous observations in which changes to ligand structure resulted in biased agonism. Note, however, that small changes to the peptide structure, such as the addition of a chemical

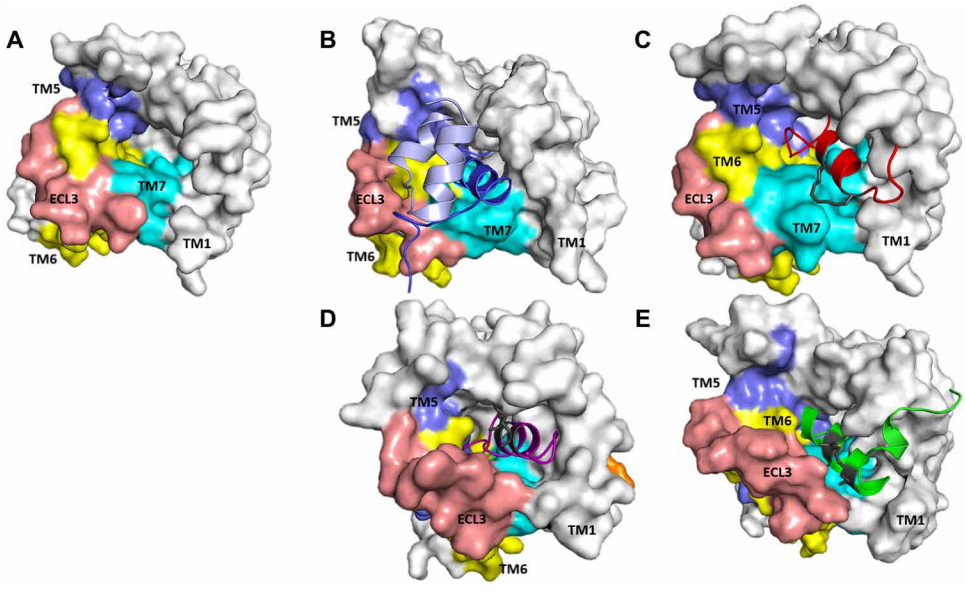

Fig. 7. Top views of the structures of Apo RXFP3 and complexes of RXFP3 with H3 relaxin and stapled peptides. (**A** to **E**) MD snapshots of the structures of (A) apo RXFP3, (B) RXFP3–H3 relaxin (the A chain and B chain are highlighted in light and dark shades of blue), (C) RXFP3–peptide 4, (D) RXFP3–d(1-7)14s18, and (E) RXFP3-14s18. In (B) and (C), the outward movement of ECL3 induced by the N-terminal region of the B chain and the stapled linker are highlighted, respectively. In (A) to (E), RXFP3 is shown as a surface with transmembrane helices (TM5 to TM7) highlighted in different colors (as for Fig. 6). The bound stapled peptides are shown as cartoons, with the staple linker highlighted as sticks in dark gray.

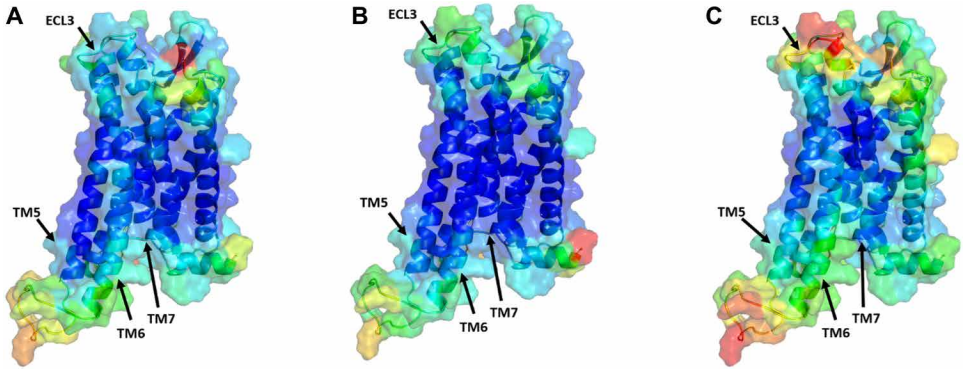

Fig. 8. Structural models of complexes formed between RXFP3 and relaxin-3 and the stapled peptides. MD snapshots of the structures of (**A**) RXFP3–H3 relaxin, (**B**) RXFP3–peptide 4, and (**C**) RXFP3-14s18. RXFP3 is shown as cartoon/surface and is colored according to flexibility (blue to red corresponds to the range of 0.5 to 9.0 Å in flexibility) as observed during the MD simulations. The peptides are omitted for clarity.

staple, may result in functional selectivity. Thus, careful study of downstream signaling pathways is essential in the early stages of peptide drug discovery. The potency and efficacy values obtained for the activation of the $G\alpha_{i/o}$ signaling and of β-arrestin1 and β-arrestin2 recruitment (Table 1) by 14s18, d(1-7)14s18, and peptide 4 showed that these ligands are partial agonists at RXFP3 compared with the full agonist, H3 relaxin. Moreover, because H3 relaxin did not activate these same signaling pathways through other endogenous receptors in WT HEK293T cells (Fig. 2, H and I), we selected H3 relaxin as the reference ligand in the bias factor calculations. Furthermore, our NanoBiT–G protein dissociation assays validated that RXFP3 primarily couples to $G\alpha_{i/o}$ over $G\alpha_s$, $G\alpha_q$, and $G\alpha_{13}$.

The pEC_{50} values for β-arrestin recruitment (Table 1) by the unbiased peptides were ~10- to 32-fold less than those for the $G\alpha_{i/o}$ activation assay. This observation is most likely due to signal amplification by the secondary messenger cAMP. Such observational and system biases were excluded in the final bias factor calculation by normalizing the responses of the partial agonists with that of the reference agonist (H3 relaxin) and obtaining $\Delta\log(\tau/K_A)$ values. The signaling bias between pathways was determined with the operational model (*39*). As the first step, transduction ratio values [$\log(\tau/K_A)$ or $\log R$] were obtained by fitting the concentration responses for the $G\alpha_{i/o}$ activation pathway and β-arrestin1/2 recruitment pathways to the operational model. Of the peptides considered in the bias factor calculations, the 14s18 and d(1-7)14s18 stapled peptides did not show a concentration response for the β-arrestin1 and β-arrestin2 recruitment assays. Thus, transduction ratio values were not determined for these peptides. Statistical analysis of the $\Delta\log(\tau/K_A)$ values for each ligand indicated that the 14s18 and d(1-7)14s18 stapled peptides varied in their relative effectiveness for each pathway compared with H3 relaxin, whereas peptide 4 was relatively similar in its effectiveness to H3 relaxin (Table 2).

Next, we used the $\Delta\log(\tau/K_A)$ to determine the signaling bias between the $G\alpha_{i/o}$ activation pathway and the β-arrestin recruitment pathways by calculating the $\Delta\Delta\log(\tau/K_A)$/bias factor (Table 3). Because $\log(\tau/K_A)$ values were absent for the recruitment of β-arrestin1/2 by 14s18 and d(1-7)14s18, bias factors were not calculated for these stapled peptides. However, if the bias factors were calculated assuming that $\log R = 0$ for the β-arrestin1/2 recruitment pathways for 14s18 and d(1-7)14s18, the bias factors may be as large as 1×10^7. In contrast, peptide 4 did not show a significant bias for the $G\alpha_{i/o}$ activation pathway or the β-arrestin1/2 recruitment pathways (Table 3). Thus, the conformational changes incurred by the position of the staple are responsible for the bias in signaling.

GPCRs recruit β-arrestin1 or β-arrestin2 in the presence of GRK2, GRK3, GRK5, or GRK6, which are the GRK subtypes most widely found in many cell types, whereas GRK1 and GRK7 are mostly associated with visual regulation (*42*–*44*). These different GRK subtypes phosphorylate the cytosolic loops and C-terminal tail of GPCRs at different residues, resulting in the generation of "bar codes" that stabilize different conformations in β-arrestins that result in differential downstream signaling (*45*, *46*). Thus, the molecular basis of the $G\alpha_{i/o}$ bias of 14s18 and d(1-7)14s18 was investigated by examining the effects of GRKs on RXFP3 upon activation by H3 relaxin or a biased stapled peptide. Our data revealed that β-arrestin recruitment to RXFP3 was mediated in the presence of GRK2 and GRK3, but not GRK5 or GRK6, in the presence of H3 relaxin (Fig. 4). However, 14s18 did not induce detectable β-arrestin recruitment in the presence of either GRK (Fig. 4). This suggests that the subsets of conformations of RXFP3 that are stabilized by the biased stapled peptide prevent the molecular events mediated by GRKs and the docking of β-arrestins. Therefore, any phosphorylation mediated by either GRK2 or GRK3 does not seem to stimulate recruitment of β-arrestin1 or β-arrestin2, or the receptor may not undergo phosphorylation, preventing β-arrestin recruitment, when RXFP3 is activated by 14s18.

The 3D structures of biased ligand–GPCR complexes have revealed the stabilization of distinct conformations (*47*, *48*). Knowledge of such conformations of RXFP3 will be useful in designing novel biased agonists and understanding the structural changes of GPCRs in biased signaling. Therefore, in the absence of the 3D structure of RXFP3, we constructed a homology model of the receptor using the crystal structure of the angiotensin II receptor in an activated state (PDB: 5XJM and PDB: 6DO1) as a template.

To build the peptide-receptor complexes in silico, the stapled peptides were generated from the nuclear magnetic resonance (NMR) solution structure of H3 relaxin (PDB: 2FHW), with staples bridging selected amino acid residues that were mutated to serines. During the 250-ns MD simulations of RXFP3 bound separately to H3 relaxin, peptide 4, and 14s18, we observed two major conformations ("open" and "closed" in ECL3) of RXFP3, which were the most populated conformations during each simulation. The unbiased peptides (relaxin-3 and peptide 4) induced an open conformation with notable movements in ECL3, TM6, and TM7 (Fig. 8), whereas the $G\alpha_{i/o}$-biased peptides did not interact with ECL3 and induced a closed conformation of the receptor. Thus, our observations suggest a previously unappreciated role for the relaxin-3 A chain, which is to interact with ECL3 and induce movements of TM6 and TM7.

Although biased peptides and the unbiased peptide 4 formed some distinct interactions with RXFP3, biased peptides interacted with different sets of amino acid residues in TM2, TM5, and TM6 during the initial binding pose. In contrast to peptide 4, the biased peptides also formed distinct interactions with TM3 and ECL3. Our studies revealed that the stapled linker of peptide 4 faces the binding site residues and interacts with RXFP3 in a manner similar to that of the A chain of H3 relaxin. Our RXFP3:H3 relaxin complex showed that the A chain of H3 relaxin is involved in supporting the interaction of the first few N-terminal residues of the B chain with ECL3. Moreover, two residues of the A-chain turn region (Ser^{16} and Lys^{17}) directly interacted with the ECL3 of RXFP3. Thus, this study assigns a previously unknown role to N-terminal residues and A chain of H3 relaxin in activating RXFP3.

Although 3D structures of the complexes of G proteins or β-arrestins complexed with RXFP3 are not available, reports on other GPCRs cocrystallized with G proteins, β-arrestins, or both suggest that structural changes at the intracellular side of these TM helices are critical in determining biased or unbiased signaling (*49*, *50*). Similarly, we speculate that the movements of TM6 and TM7 observed at the intracellular side of RXFP3 bound to peptide 4 and 14s18 or d(1-7)14s18 could regulate the unbiased versus biased signaling of RXFP3. Active state crystal structures of β2 adrenergic receptor (β_2AR), rhodopsin, adenosine receptor A_{2a}R, muscarinic M_2 receptor (M_2R), and μ-opioid receptors revealed major outward moments in the inner module of TM6 that facilitate G protein binding (*51*–*57*). For β_2AR, displacement of TM5 and TM7 was also observed, and these positional changes generate a more open conformation in the cytoplasmic domain to generate the binding pocket that consists of residues of TM3, TM5, and TM6 for the docking of the G protein α subunit. According to cocrystallized structures with

β-arrestins, the involvement of TM7, helix 8, and intracellular loop 1 (ICL1) domains together with G protein–binding sites has been observed for β-arrestin recruitment to rhodopsin, neurotensin receptor 1, β_1AR, and M_2R (*58*–*61*).

A study of the μ-opioid receptor proposed that distinct, closed conformations in TM7, helix 8, and ICL1 induced by the inward moment of TM7 upon the binding of a G protein–biased ligand might restrain the binding of β-arrestin to the receptor (*62*). Previous fluorescence-based studies of arginine–vasopressin type 2 receptor (V_2R) revealed that the specific movements of TM3 and ICL3 and the movements of TM7 and helix 8 are involved in G protein–specific and β-arrestin–specific biased ligand binding, respectively (*63*). A distinct conformation in TM7 was also observed in an F-NMR study of β_2AR interacting with a β-arrestin–biased ligand (*64*). Similarly, we speculate that the movements of TM6 and TM7 observed at the intracellular side of RXFP3 bound to the unbiased peptides H3 relaxin and peptide 4 and the biased peptides 14s18 and d(1-7)14s18 could determine whether signaling by RXFP3 is biased or not. Furthermore, structural modeling of the ternary complex between the stapled peptide, RXFP3, and a G protein or β-arrestin will likely result in a greater understanding of biased versus unbiased signaling resulting from the stapled peptides peptide 4, 14s18, and d(1-7)14s18.

Upon confirming the occurrence of biased signaling and the molecular and structural properties that immediately proceed after ligand binding, we then explored the effects on the downstream signaling pathways of RXFP3, such as ERK1/2 activation, which is partially modulated by β-arrestin recruitment followed by endocytosis of RXFP3 (*40*, *41*). Moreover, SRE reporter gene activation is preceded by the activation of ETS like-1 protein (Elk-1) and ERK1/2 (*65*). Compared with H3 relaxin, 14s18 and d(1-7)14s18 displayed reduced potencies in the ERK1/2 activation assays and even lower potencies in the SRE reporter gene activation assay, indicating considerably reduced effectiveness in these pathways. This suggests that the bias and changes in the receptor conformation may result in variable phenotypes. However, further studies by solution NMR, x-ray crystallography, or cryo–electron microscopy to confirm these conformational changes could provide further evidence of the structural changes described earlier. Moreover, in vivo studies to assess the phenotypic relevance of the biased peptides could shed light on the molecular mechanisms underlying these phenotypes. The importance of G protein activation by RXFP3 was reported in a study performed with rat brain slices, which demonstrated pertussis toxin (PTX)–dependent inhibition of the inhibitory action of RXFP3-A2 on oxytocin and vasopressin neurons in the paraventricular nucleus of the hypothalamus. This suggests that the orexigenic action of relaxin-3 is mediated by $G\alpha_{i/o}$ activation (*66*). Moreover, the $G\alpha_{i/o}$ pathway mediates the orexigenic activity of hypothalamic neuropeptides, such as neuropeptide Y (NPY) (*67*–*69*) and nesfatin-1 (*70*) in rat brains. In addition, inhibition of the $G\alpha_{i/o}$ pathway by PTX blocks feeding behavior in *Drosophila* (*71*). Thus, a $G\alpha_{i/o}$-biased ligand will be an excellent tool to study the orexigenic activity mediated by RXFP3 without perturbing other pathways activated by an unbiased RXFP3 agonist. Furthermore, a $G\alpha_{i/o}$-biased agonist of RXFP3 will be an important candidate in targeting feeding disorders mediated by the relaxin-3/RXFP3 system. The lack of β-arrestin recruitment affects GPCR trafficking, resulting in reduced receptor desensitization. Therefore, this may have a profound effect on signal stability, particularly in vivo.

In conclusion, we have revealed that the position of the staple of the 14s18 and d(1-7)14s18 peptides prevented the staple from interacting with RXFP3, rendering the peptides to be $G\alpha_{i/o}$-biased ligands of the receptor. The distinct conformations of RXFP3 stabilized by these peptides prevented GRK2- and GRK3-mediated β-arrestin1/2 recruitment, in contrast with the effects of H3 relaxin. Moreover, these peptides showed reduced potency in ERK1/2 activation and SRE reporter gene activation compared with the unbiased ligand H3 relaxin. However, peptide 4, which is a truncated H3 relaxin B-chain hydrocarbon stapled at the 13 to 17 positions, did not show bias toward G protein activation or β-arrestin recruitment to RXFP3. Conformational changes in ECL3, TM6, and TM7 of RXFP3 may be required to stimulate β-arrestin1 and β-arrestin2 recruitment. Last, these findings also suggest a previously uncharacterized role of the relaxin-3 A chain and the N-terminal region of the B chain in promoting movements in ECL3, TM6, and TM7 that induce the formation of an open conformation of RXFP3 at the cytosolic side, which is possibly associated with β-arrestin1 and β-arrestin2 recruitment to RXFP3.

MATERIALS AND METHODS

Cell culture

HEK-RXFP3 cells were provided by R. Bathgate (Florey Institute of Neuroscience and Mental Health, University of Melbourne). WT HEK293T cells were provided by L. Stanton (Genome Institute of Singapore). HEK-RXFP3 and HEK293T cells were maintained in Dulbecco's modified Eagle's medium (DMEM; Life Technologies) in 10% (v/v) fetal bovine serum (FBS; Life Technologies) and 1× penicillin-streptomycin (Life Technologies) at 37°C in a 5% CO_2 humidified environment. Both cell lines were passaged with TrypLE Express (Life Technologies) at 80% confluency.

Peptides

The hydrocarbon-stapled peptides, 14s18 (*36*), d(1-7)14s18, peptide 4 (*35*), and H3 relaxin B chain analogs were synthesized and purified by Biosynthesis Inc. As previously described, amino acids at the i and i+4 positions were substituted with (*S*)2-(4′-pentenyl)alanine, which was followed by RCM during the synthesis of the stapled peptides (*36*). The d(1-7)14s18 stapled peptide was designed by eliminating the first seven residues of the H3 relaxin B chain because they do not contribute to binding and activating RXFP3 (*11*). H3 relaxin was purchased from Phoenix Pharmaceuticals.

NanoBiT–G protein dissociation assay

The G proteins that interacted with RXFP3 upon activation by H3 relaxin and 14s18 were determined using a previously established NanoBiT–G protein dissociation assay (*72*).

ELISA-based cAMP assay

Activation of $G\alpha_{i/o}$ was determined with an assay by measuring the inhibition of forskolin-induced cAMP production, which was optimized as previously described with a cAMP EIA kit (Cayman Chemicals) (*36*). To generate concentration-response curves, H3 relaxin (1 pM to 100 nM), B chain DM (1 pM to 10 μM), 14s18 (1 pM to 10 μM), d(1-7)14s18 (1 pM to 10 μM), Peptide 4 (1 pM to 10 μM), and d(1-7)B chain DM (1 pM to 10 μM) were

applied in parallel with the vehicle control to HEK-RXFP3 cells and HEK293T cells in triplicate in three or four independent experiments.

NanoBiT β-arrestin recruitment assay

The NanoBiT β-arrestin assay was performed as described previously (*73*). The pCAGGS-LgBiT-ARRB1 [large fragment (LgBiT) N-terminally fused to β-arrestin1; LgBiT was gene-synthesized by Genscript with codon optimization], pCAGGS-LgBiT-ARRB2 [large fragment (LgBiT) N-terminally fused to β-arrestin2], and human RXFP3 coding sequence containing (accession no. NM_016568) pCAGGS-RXFP3-SmBiT [small fragment (SmBiT) C-terminally fused to RXFP3 with a 15–amino acid flexible linker; GGSGGGGS-GGSSSGGVTGYRLFEEIL] were constructed. To optimize the transfection conditions, HEK293 cells were plated in a six-well plate (4×10^5 cells per well) with DMEM supplemented with 10% fetal calf serum (FCS) and penicillin and streptomycin. After 1 day of incubation at 37°C with 5% CO_2, the cells were cotransfected with combinations of 100, 200, and 500 ng of pCAGGS-LgBiT-ARRB1, pCAGGS-LgBiT-ARRB2, pCAGGS-RXFP3-SmBiT, and pCAGGS (empty vector) with Lipofectamine 2000. The following day, the cells were trypsinized with 0.53 mM Dulbecco's phosphate-buffered saline–EDTA and plated in a white, 96-well plate (6.4×10^4 cells per well) with Hanks' balanced salt solution (HBSS) supplemented with 0.01% bovine serum albumin (BSA) and 5 mM Hepes. Immediately after plating, coelenterazine or coelenterazine h (Wako Pure Chemical) was added to the wells to a final concentration of 10 μM and incubated at room temperature for 2 hours. At the end of the incubation, initial luminescence measurement was obtained, and the cells were treated with vehicle or 10 nM H3 relaxin, followed by continuous luminescence measurement for 15 min with a SpectraMax L plate reader (Molecular Devices). For the generation of concentration-response curves, HEK293T cells were plated in six-well plates (at 4×10^5 cells per well) that were coated with poly-L-lysine (Sigma-Aldrich) and incubated with DMEM supplemented with 10% FBS and penicillin-streptomycin. On the next day, cells were transfected with pCAGGS-LgBiT-ARRB1 (100 ng per well) and pCAGGS-RXFP3-SmBiT (200 ng per well) for experiments to quantify β-arrestin1 recruitment to activated RXFP3 or with pCAGGS-LgBiT-ARRB2 (100 ng per well) and pCAGGS-RXFP3-SmBiT (200 ng per well) for experiments to quantify β-arrestin2 recruitment to activated RXFP3 and were assayed as described earlier. Treatment with H3 relaxin was performed with six concentrations (1 pM to 100 nM) each in triplicate, and 14s18, d(1-7)14s18, Peptide 4, B chain DM, and d(1-7)B chain DM were applied at eight concentrations (1 pM to 10 μM). To determine GRK subtype bias, we performed experiments with GRK2/3/5/6 knockout cells and determined β-arrestin1/2 recruitment to RXFP3 upon GRK add-back with either H3 relaxin or 14s18, according to a previously reported method (*74*).

HTRF ERK1/2 activation assay

Activation of ERK1/2 in HEK-RXFP3 cells was measured by an HTRF-based assay (phospho-ERK1/2, Cisbio Bioassays, Codolet France). Briefly, HEK-RXFP3 cells (50,000 per well) were plated in DMEM, 10% FBS, and penicillin and streptomycin in the inner wells of poly-L-lysine–coated, 96-well plates. Next, the cells were serum-starved overnight. During the optimizations, the cells were treated with 1 pM, 500 pM, or 100 nM H3 relaxin or with vehicle or 10% FBS (positive control) for 8 min, after which the medium was discarded, and the cells were lysed with 25 μl of 1× lysis buffer for 1 or 2 hours at 150 rpm at room temperature. Here, 10% FBS was used as a positive control because it activates the mitogen-activated protein kinase (MAPK) pathway (*75*–*78*). At the end of cell lysis, 16 μl of cell lysate was transferred into 384-half-area-well plates (Greiner Bio-One, Germany) and assayed according to the manufacturer's instructions. To generate concentration-response curves, H3 relaxin (1 pM to 100 nM), 14s18 (1 pM to 10 μM), and d(1-7)14s18 (1 pM to 10 μM) were applied in parallel with the vehicle and 10% FBS (positive control) on HEK-RXFP3 cells in triplicate, and the assay was performed using the optimized conditions. The experiments were performed three times.

Luciferase *SRE* reporter gene activation assay

SRE reporter gene activation was measured by a luciferase reporter gene assay. To determine the time course of SRE reporter gene activation, HEK-RXFP3 cells were reverse-transfected with 100 ng of pGL4.33[*luc2P*/SRE/Hygro] plasmids per well with Lipofectamine 2000 reagent (Life Technologies) and plated in the inner wells of poly-L-lysine–coated, white 96-well plates with DMEM supplemented with 10% FBS. One day after the transfection, cells were serum-starved overnight. After starvation, cells were treated with 100 nM H3 relaxin for 2, 4, 6, 12, 18, and 24 hours, which was followed by lysing the cells with ONE-Glo luciferase assay substrate (Promega). The luminescence was measured with a Tecan Spark microplate reader. To optimize the transfection conditions, HEK-RXFP3 cells (10,000 cells per well) were reverse-transfected with 100, 200, or 500 ng of pGL4.33[*luc2P*/SRE/Hygro] plasmids with Lipofectamine 2000 reagent and plated with DMEM supplemented with 10% FBS in the inner wells of poly-L-lysine–coated, white 96-well plates. One day after the transfection, the cells were serum-starved overnight. After starvation, cells were treated with H3 relaxin (1 pM to 100 nM) for 4 hours and assayed as described earlier. To generate concentration-response curves, H3 relaxin (1 pM to 100 nM), 14s18 (1 pM to 10 μM), and d(1-7)14s18 (1 pM to 10 μM) stapled peptides were applied in parallel with the vehicle and 10% FBS (positive control) on HEK-RXFP3 cells in six replicates per experiment. Experiments were performed three times.

In silico modeling of RXFP3–stapled peptide interactions

A homology model of RXFP3 was constructed using the crystal structure of the angiotensin II receptor in an activated state (PDB: 5XJM and PDB: 6DO1) as a template. The structures of the stapled peptides [peptide 4, 14s18, and d(1-7)14s18] were constructed from the NMR solution structure of H3 relaxin (PDB: 2FHW), each with staples bridging different positions (13 to 17 and 14 to 18) and modeled. Structural models of the bound state of H3 relaxin onto RXFP3 were generated with the program Modeller 9v18 (*79*) using distance restraints corresponding to mutational data. In addition to building models of the two stapled peptides bound to RXFP3, we also modeled the complex between RXFP3 and H3 relaxin, for which the NMR structure of H3 relaxin (PDB: 2FHW) was used. The generated models of peptide/H3 relaxin complexed to RXFP3 were next embedded in the model of a membrane composed of POPC (1-palmitoyl-2-oleoyl-sn-glycero-3-phosphocholine)/POPE (1-palmitoyl-2-oleoyl phosphatidylethanolamine)/cholesterol molecules (60:20:20); all complexes were further refined by MD simulations. MD simulations were performed with the pmemd.

CUDA module of the program Amber18 (*80*). All atom versions of the Amber 14SB force field (ff14SB) (*81*) and the AMBER lipid14 force field (*82*) were used to model the protein and membrane, respectively. The Xleap module of Amber was used to prepare the system for the MD simulations. Each simulation system was neutralized with an appropriate number of counterions. Each neutralized system was solvated with TIP3P (*83*) water molecules. Solvent molecules and counterions were initially relaxed using energy minimization with restraints on the protein atoms. This was followed by unrestrained energy minimization to remove any steric clashes. Subsequently, the system was gradually heated from 0 to 300 K with MD simulations with positional restraints (force constant: 50 kcal mol^{-1} $Å^{-2}$) on the receptor and peptides over a period of 0.25 ns, enabling water molecules and ions to move freely. During an additional 0.25 ns, the positional restraints were gradually reduced, which was followed by a 10-ns unrestrained MD simulation to equilibrate all of the atoms. During the simulations, Lennard-Jones and short-range electrostatic interactions were treated with a cutoff scheme, and the long-range electrostatic interactions were treated with the particle mesh Ewald method (*84*) using a real space cutoff distance of 9 Å. The Settle (*85*) algorithm was used to constrain bond vibrations involving hydrogen atoms, which enabled a time step of 2 fs during the simulations. The Langevin thermostat with a damping coefficient of 2.0 ps^{-1} and the Berendsen barostat with a coupling time constant of 1.0 ps were used to maintain pressure and temperature. For each system, 250-ns production MD runs at 300 K in triplicate (assigning different initial velocities) were performed. Simulation trajectories were visualized with VMD (*86*), and figures were generated with Pymol (*87*).

Data analysis

In the cAMP ELISA assay, the cAMP concentrations were calculated using a cAMP standard curve (0.3 to 750 nM) (*36*). In the NanoBiT enzyme complementation assay, luminescence after ligand or vehicle treatment was normalized by the initial luminescence. Normalized values were then plotted against time (in minutes) in GraphPad Prism to obtain the area under the curve (AUC) for each treatment type. In the HTRF ERK1/2 assay and the luciferase assay, the fluorescence and luminescence values of the H3 relaxin–treated samples were normalized and represented as a percentage of the average response to 10% FBS. For the forskolin-induced inhibition of cAMP production assay, the NanoBiT enzyme complementation assay, and the SRE reporter gene activation assay, data were normalized and presented as a percentage of the maximal H3 relaxin–stimulated response in each independent experiment. The normalized responses were analyzed with nonlinear curve fitting [four-parameter Hill equation: $Y = \text{Bottom} + (\text{Top} - \text{Bottom})/(1 + 10\text{^}(\log EC_{50} - X))$] with GraphPad Prism V.5 software to estimate the pEC_{50} and E_{max} values from the concentration-response curves. Ligand bias was quantified as previously described with the operational model of agonism (*88*–*91*). Briefly, concentration-response values from the cAMP and β-arrestin recruitment assays expressed as percentages of the maximal H3 relaxin–stimulated response were fitted into Eq. 1 (*88*) derived from the standard form of the operational model (*39*) to determine the transduction ratios (τ/K_A) with GraphPad Prism V.5 software. In this equation, ε is the effect of the ligand, [A] is the agonist concentration, ε_m is the maximum response of the system, Basal indicates the basal response at the absence of the agonist, K_A indicates the functional equilibrium dissociation constant of the agonist, n denotes the transducer function slope that links occupancy to the response, and log$R$ is the logarithm of the transduction coefficient/ratio also denoted by $\log(\tau/K_A)$, where τ represents an index of the coupling efficiency (*88*).

$$\varepsilon = \text{Basal} + \frac{(\varepsilon_m - \text{Basal})}{1 + ((([A]/10^{\log K_A}) + 1)/(10^{\log K_X}[A]))^n} \quad (1)$$

Next, to eliminate system and observational bias, transduction ratio values for the peptides were compared with that of the reference ligand (H3 relaxin) to obtain the relative effectiveness of the peptide toward a certain signaling pathway by Eqs. 2 and 3

$$\Delta\log(\tau/K_A) = \log(\tau/K_A)_{\text{LIGAND}} - \log(\tau/K_A)_{\text{H3 relaxin}} \quad (2)$$

$$\text{Relative effectiveness (RE)} = 10^{\Delta\log(\tau/K_A)} \quad (3)$$

Ligand bias, the difference between $\Delta\log(\tau/K_A)$ ratios between two pathways, was calculated using the following equations

$$\Delta\Delta\log(\tau/K_A) = \Delta\log(\tau/K_A)_{\text{LIGAND1,Pathway1}} - \Delta\log(\tau/K_A)_{\text{LIGAND2,Pathway2}} \quad (4)$$

$$\text{Bias factor} = 10^{\Delta\Delta\log(\tau/K_A)} \quad (5)$$

Supplementary Materials

This PDF file includes:

Figs. S1 to S5

Other Supplementary Material for this manuscript includes the following:

PDB files
MDAR Reproducibility Checklist
Data files S1 to S3

REFERENCES AND NOTES

1. F. Shabanpoor, F. Separovic, J. D. Wade, Chapter 1 The human insulin superfamily of polypeptide hormones. *Vitam. Horm.* **80**, 1–31 (2009).
2. K. J. Rosengren, F. Lin, R. A. D. Bathgate, G. W. Tregear, N. L. Daly, J. D. Wade, D. J. Craik, Solution structure and novel insights into the determinants of the receptor specificity of human relaxin-3. *J. Biol. Chem.* **281**, 5845–5851 (2006).
3. R. A. Bathgate, R. Ivell, B. M. Sanborn, O. D. Sherwood, R. J. Summers, International Union of Pharmacology LVII: Recommendations for the nomenclature of receptors for relaxin family peptides. *Pharmacol. Rev.* **58**, 7–31 (2006).
4. C. Liu, E. Eriste, S. Sutton, J. Chen, B. Roland, C. Kuei, N. Farmer, H. Jörnvall, R. Sillard, T. W. Lovenberg, Identification of relaxin-3/INSL7 as an endogenous ligand for the orphan G-protein-coupled receptor GPCR135. *J. Biol. Chem.* **278**, 50754–50764 (2003).
5. M. Goto, L. W. Swanson, N. S. Canteras, Connections of the nucleus incertus. *J. Comp. Neurol.* **438**, 86–122 (2001).
6. S. Ma, P. Bonaventure, T. Ferraro, P.-J. Shen, T. C. D. Burazin, R. A. D. Bathgate, C. Liu, G. W. Tregear, S. W. Sutton, A. L. Gundlach, Relaxin-3 in GABA projection neurons of nucleus incertus suggests widespread influence on forebrain circuits via G-protein-coupled receptor-135 in the rat. *Neuroscience* **144**, 165–190 (2007).
7. R. A. D. Bathgate, C. S. Samuel, T. C. D. Burazin, S. Layfield, A. A. Claasz, I. G. T. Reytomas, N. F. Dawson, C. Zhao, C. Bond, R. J. Summers, L. J. Parry, J. D. Wade, G. W. Tregear, Human relaxin gene 3 (*H3*) and the equivalent mouse relaxin (*M3*) gene: Novel members of the relaxin peptide family. *J. Biol. Chem.* **277**, 1148–1157 (2002).
8. S. Ma, C. M. Smith, A. Blasiak, A. L. Gundlach, Distribution, physiology and pharmacology of relaxin-3/RXFP3 systems in brain. *Br. J. Pharmacol.* **174**, 1034–1048 (2017).
9. S. Sudo, J. Kumagai, S. Nishi, S. Layfield, T. Ferraro, R. A. D. Bathgate, A. J. W. Hsueh, H3 relaxin is a specific ligand for LGR7 and activates the receptor by interacting with both the ectodomain and the exoloop 2. *J. Biol. Chem.* **278**, 7855–7862 (2003).

10. C. Liu, J. Chen, S. Sutton, B. Roland, C. Kuei, N. Farmer, R. Sillard, T. W. Lovenberg, Identification of relaxin-3/INSL7 as a ligand for GPCR142. *J. Biol. Chem.* **278**, 50765–50770 (2003).
11. C. Kuei, S. Sutton, P. Bonaventure, C. Pudiak, J. Shelton, J. Zhu, D. Nepomuceno, J. Wu, J. Chen, F. Kamme, M. Seierstad, M. D. Hack, R. A. D. Bathgate, M. A. Hossain, J. D. Wade, J. Atack, T. W. Lovenberg, C. Liu, R3(BΔ23–27)R/I5 chimeric peptide, a selective antagonist for GPCR135 and GPCR142 over relaxin receptor LGR7: In vitro and in vivo characterization. *J. Biol. Chem.* **282**, 25425–25435 (2007).
12. M. A. Hossain, K. J. Rosengren, L. M. Haugaard-Jönsson, S. Zhang, S. Layfield, T. Ferraro, N. L. Daly, G. W. Tregear, J. D. Wade, R. A. D. Bathgate, The A-chain of human relaxin family peptides has distinct roles in the binding and activation of the different relaxin family peptide receptors. *J. Biol. Chem.* **283**, 17287–17297 (2008).
13. F. Shabanpoor, M. A. Hossain, P. J. Ryan, A. Belgi, S. Layfield, M. Kocan, S. Zhang, C. S. Samuel, A. L. Gundlach, R. A. D. Bathgate, F. Separovic, J. D. Wade, Minimization of human relaxin-3 leading to high-affinity analogues with increased selectivity for relaxin-family peptide 3 receptor (RXFP3) over RXFP1. *J. Med. Chem.* **55**, 1671–1681 (2012).
14. J. R. Kumar, R. Rajkumar, T. Jayakody, S. Marwari, J. M. Hong, S. Ma, A. L. Gundlach, M. K. P. Lai, G. S. Dawe, Relaxin' the brain: A case for targeting the nucleus incertus network and relaxin-3/RXFP3 system in neuropsychiatric disorders. *Br. J. Pharmacol.* **174**, 1061–1076 (2016).
15. A. Banerjee, P.-J. Shen, S. Ma, R. A. D. Bathgate, A. L. Gundlach, Swim stress excitation of nucleus incertus and rapid induction of relaxin-3 expression via CRF_1 activation. *Neuropharmacology* **58**, 145–155 (2010).
16. Y. Watanabe, Y. Miyamoto, T. Matsuda, M. Tanaka, Relaxin-3/INSL 7 regulates the stress-response system in the rat hypothalamus. *J. Mol. Neurosci.* **43**, 169–174 (2011).
17. M. Tanaka, N. Iijima, Y. Miyamoto, S. Fukusumi, Y. Itoh, H. Ozawa, Y. Ibata, Neurons expressing relaxin 3/INSL 7 in the nucleus incertus respond to stress. *Eur. J. Neurosci.* **21**, 1659–1670 (2005).
18. B. M. McGowan, J. S. Minnion, K. G. Murphy, D. Roy, S. A. Stanley, W. S. Dhillo, J. V. Gardiner, M. A. Ghatei, S. R. Bloom, Relaxin-3 stimulates the neuro-endocrine stress axis via corticotrophin-releasing hormone. *J. Endocrinol.* **221**, 337–346 (2014).
19. C. Zhang, B. E. Chua, A. Yang, F. Shabanpoor, M. A. Hossain, J. D. Wade, K. J. Rosengren, C. M. Smith, A. L. Gundlach, Central relaxin-3 receptor (RXFP3) activation reduces elevated, but not basal, anxiety-like behaviour in C57BL/6J mice. *Behav. Brain Res.* **292**, 125–132 (2015).
20. S. Marwari, A. Poulsen, N. Shih, R. Lakshminarayanan, R. M. Kini, C. W. Johannes, B. W. Dymock, G. S. Dawe, Intranasal administration of a stapled relaxin-3 mimetic has anxiolytic- and antidepressant-like activity in rats. *Br. J. Pharmacol.* **176**, 3899–3923 (2019).
21. V. Rytova, D. E. Ganella, D. Hawkes, R. A. D. Bathgate, S. Ma, A. L. Gundlach, Chronic activation of the relaxin-3 receptor on GABA neurons in rat ventral hippocampus promotes anxiety and social avoidance. *Hippocampus* **29**, 905–920 (2019).
22. B. M. C. McGowan, S. A. Stanley, K. L. Smith, N. E. White, M. M. Connolly, E. L. Thompson, J. V. Gardiner, K. G. Murphy, M. A. Ghatei, S. R. Bloom, Central relaxin-3 administration causes hyperphagia in male Wistar rats. *Endocrinology* **146**, 3295–3300 (2005).
23. B. M. McGowan, S. A. Stanley, K. L. Smith, J. S. Minnion, J. Donovan, E. L. Thompson, M. Patterson, M. M. Connolly, C. R. Abbott, C. J. Small, J. V. Gardiner, M. A. Ghatei, S. R. Bloom, Effects of acute and chronic relaxin-3 on food intake and energy expenditure in rats. *Regul. Pept.* **136**, 72–77 (2006).
24. S. W. Sutton, J. Shelton, C. Smith, J. Williams, S. Yun, T. Motley, C. Kuei, P. Bonaventure, A. Gundlach, C. Liu, T. Lovenberg, Metabolic and neuroendocrine responses to RXFP3 modulation in the central nervous system. *Ann. N. Y. Acad. Sci.* **1160**, 242–249 (2009).
25. C. Lenglos, A. Mitra, G. Guèvremont, E. Timofeeva, Regulation of expression of relaxin-3 and its receptor RXFP3 in the brain of diet-induced obese rats. *Neuropeptides* **48**, 119–132 (2014).
26. J. Munro, O. Skrobot, M. Sanyoura, V. Kay, M. T. Susce, P. E. A. Glaser, J. de Leon, A. I. F. Blakemore, M. J. Arranz, Relaxin polymorphisms associated with metabolic disturbance in patients treated with antipsychotics. *J. Psychopharmacol.* **26**, 374–379 (2012).
27. H. Yamamoto, H. Shimokawa, T. Haga, Y. Fukui, K. Iguchi, K. Unno, M. Hoshino, A. Takeda, The expression of relaxin-3 in adipose tissue and its effects on adipogenesis. *Protein Pept. Lett.* **21**, 517–522 (2014).
28. R. Rajkumar, L. K. Y. See, G. S. Dawe, Acute antipsychotic treatments induce distinct c-Fos expression patterns in appetite-related neuronal structures of the rat brain. *Brain Res.* **1508**, 34–43 (2013).
29. A. Kania, A. Szlaga, P. Sambak, A. Gugula, E. Blasiak, M. V. M. Di Bonaventura, M. A. Hossain, C. Cifani, G. Hess, A. L. Gundlach, A. Blasiak, RLN3/RXFP3 signaling in the PVN inhibits magnocellular neurons via M-like current activation and contributes to binge eating behavior. *J. Neurosci.* **40**, 5362–5375 (2020).
30. S. Ma, F. E. Olucha-Bordonau, M. A. Hossain, F. Lin, C. Kuei, C. Liu, J. D. Wade, S. W. Sutton, A. Nuñez, A. L. Gundlach, Modulation of hippocampal theta oscillations and spatial memory by relaxin-3 neurons of the nucleus incertus. *Learn. Mem.* **16**, 730–742 (2009).
31. S. Ma, A. Blasiak, F. E. Olucha-Bordonau, A. J. M. Verberne, A. L. Gundlach, Heterogeneous responses of nucleus incertus neurons to corticotrophin-releasing factor and coherent activity with hippocampal theta rhythm in the rat. *J. Physiol.* **591**, 3981–4001 (2013).
32. A. Belgi, R. A. D. Bathgate, M. Kocan, N. Patil, S. Zhang, G. W. Tregear, J. D. Wade, M. A. Hossain, Minimum active structure of insulin-like peptide 5. *J. Med. Chem.* **56**, 9509–9516 (2013).
33. T. Kenakin, Agonist-receptor efficacy II: Agonist trafficking of receptor signals. *Trends Pharmacol. Sci.* **16**, 232–238 (1995).
34. J. D. Urban, W. P. Clarke, M. von Zastrow, D. E. Nichols, B. Kobilka, H. Weinstein, J. A. Javitch, B. L. Roth, A. Christopoulos, P. M. Sexton, K. J. Miller, M. Spedding, R. B. Mailman, Functional selectivity and classical concepts of quantitative pharmacology. *J. Pharmacol. Exp. Ther.* **320**, 1–13 (2007).
35. K. Hojo, M. A. Hossain, J. Tailhades, F. Shabanpoor, L. L. L. Wong, E. E. K. Ong-Pålsson, H. E. Kastman, S. Ma, A. L. Gundlach, K. J. Rosengren, J. D. Wade, R. A. D. Bathgate, Development of a single-chain peptide agonist of the relaxin-3 receptor using hydrocarbon stapling. *J. Med. Chem.* **59**, 7445–7456 (2016).
36. T. Jayakody, S. Marwari, R. Lakshminarayanan, F. C. K. Tan, C. W. Johannes, B. W. Dymock, A. Poulsen, D. R. Herr, G. S. Dawe, Hydrocarbon stapled B chain analogues of relaxin-3 retain biological activity. *Peptides* **84**, 44–57 (2016).
37. G. S. Dawe, T. Jayakody, S. Mawari, Stapled B chain analogues of relaxin-3 retain biological activity. *FASEB J.* **30**, lb512 (2016).
38. E. A. Gay, J. D. Urban, D. E. Nichols, G. S. Oxford, R. B. Mailman, Functional selectivity of D_2 receptor ligands in a Chinese hamster ovary hD_{2L} cell line: Evidence for induction of ligand-specific receptor states. *Mol. Pharmacol.* **66**, 97–105 (2004).
39. J. W. Black, P. Leff, Operational models of pharmacological agonism. *Proc. R. Soc. Lond. B Biol. Sci.* **220**, 141–162 (1983).
40. M. Kocan, M. Sarwar, M. A. Hossain, J. D. Wade, R. J. Summers, Signalling profiles of H3 relaxin, H2 relaxin and R3(BΔ23–27)R/I5 acting at the relaxin family peptide receptor 3 (RXFP3). *Br. J. Pharmacol.* **171**, 2827–2841 (2014).
41. E. T. van der Westhuizen, T. D. Werry, P. M. Sexton, R. J. Summers, The relaxin family peptide receptor 3 activates extracellular signal-regulated kinase 1/2 through a protein kinase C-dependent mechanism. *Mol. Pharmacol.* **71**, 1618–1629 (2007).
42. R. Sterne-Marr, J. L. Benovic, Regulation of G protein-coupled receptors by receptor kinases and arrestins. *Vitam. Horm.* **51**, 193–234 (1995).
43. O. Hisatomi, S. Matsuda, T. Satoh, S. Kotaka, Y. Imanishi, F. Tokunaga, A novel subtype of G-protein-coupled receptor kinase, GRK7, in teleost cone photoreceptors. *FEBS Lett.* **424**, 159–164 (1998).
44. J. A. Pitcher, N. J. Freedman, R. J. Lefkowitz, G protein-coupled receptor kinases. *Annu. Rev. Biochem.* **67**, 653–692 (1998).
45. Q. Liu, Q.-T. He, X. Lyu, F. Yang, Z.-L. Zhu, P. Xiao, Z. Yang, F. Zhang, Z.-Y. Yang, X.-Y. Wang, P. Sun, Q.-W. Wang, C.-X. Qu, Z. Gong, J.-Y. Lin, Z. Xu, S.-L. Song, S.-M. Huang, S.-C. Guo, M.-J. Han, K.-K. Zhu, X. Chen, A. W. Kahsai, K.-H. Xiao, W. Kong, F.-H. Li, K. Ruan, Z.-J. Li, X. Yu, X.-G. Niu, C.-W. Jin, J. Wang, J.-P. Sun, DeSiphering receptor core-induced and ligand-dependent conformational changes in arrestin via genetic encoded trimethylsilyl ^{1}H-NMR probe. *Nat. Commun.* **11**, 4857 (2020).
46. H. Chen, S. Zhang, X. Zhang, H. Liu, QR code model: A new possibility for GPCR phosphorylation recognition. *Cell Commun. Signal.* **20**, 23 (2022).
47. S. Peddibhotla, M. P. Hedrick, P. Hershberger, P. R. Maloney, Y. Li, M. Milewski, P. Gosalia, W. Gray, A. Mehta, E. Sugarman, B. Hood, E. Suyama, K. Nguyen, S. Heynen-Genel, S. Vasile, S. Salaniwal, D. Stonich, Y. Su, A. Mangravita-Novo, M. Vicchiarelli, G. P. Roth, L. H. Smith, T. D. Y. Chung, G. R. Hanson, J. B. Thomas, M. G. Caron, L. S. Barak, A. B. Pinkerton, Discovery of ML314, a brain penetrant nonpeptidic β-arrestin biased agonist of the neurotensin NTR1 receptor. *ACS Med. Chem. Lett.* **4**, 846–851 (2013).
48. T. Evron, S. M. Peterson, N. M. Urs, Y. Bai, L. K. Rochelle, M. G. Caron, L. S. Barak, G protein and β-Arrestin signaling bias at the ghrelin receptor. *J. Biol. Chem.* **289**, 33442–33455 (2014).
49. L. M. Wingler, M. Elgeti, D. Hilger, N. R. Latorraca, M. T. Lerch, D. P. Staus, R. O. Dror, B. K. Kobilka, W. L. Hubbell, R. J. Lefkowitz, Angiotensin analogs with divergent bias stabilize distinct receptor conformations. *Cell* **176**, 468–478.e11 (2019).
50. A. Manglik, T. H. Kim, M. Masureel, C. Altenbach, Z. Yang, D. Hilger, M. T. Lerch, T. S. Kobilka, F. S. Thian, W. L. Hubbell, R. S. Prosser, B. K. Kobilka, Structural insights into the dynamic process of β2-adrenergic receptor signaling. *Cell* **161**, 1101–1111 (2015).
51. S. G. F. Rasmussen, H.-J. Choi, J. J. Fung, E. Pardon, P. Casarosa, P. S. Chae, B. T. De Vree, D. M. Rosenbaum, F. S. Thian, T. S. Kobilka, A. Schnapp, I. Konetzki, R. K. Sunahara, S. H. Gellman, A. Pautsch, J. Steyaert, W. I. Weis, B. K. Kobilka, Structure of a nanobody-stabilized active state of the β_2 adrenoceptor. *Nature* **469**, 175–180 (2011).

52. A. M. Ring, A. Manglik, A. C. Kruse, M. D. Enos, W. I. Weis, K. C. Garcia, B. K. Kobilka, Adrenaline-activated structure of β_2-adrenoceptor stabilized by an engineered nanobody. *Nature* **502**, 575–579 (2013).
53. H.-W. Choe, Y. J. Kim, J. H. Park, T. Morizumi, E. F. Pai, N. Krauss, K. P. Hofmann, P. Scheerer, O. P. Ernst, Crystal structure of metarhodopsin II. *Nature* **471**, 651–655 (2011).
54. J. Standfuss, P. C. Edwards, A. D'Antona, M. Fransen, G. Xie, D. D. Oprian, G. F. X. Schertler, The structural basis of agonist-induced activation in constitutively active rhodopsin. *Nature* **471**, 656–660 (2011).
55. B. Carpenter, R. Nehmé, T. Warne, A. G. W. Leslie, C. G. Tate, Structure of the adenosine A_{2A} receptor bound to an engineered G protein. *Nature* **536**, 104–107 (2016).
56. A. C. Kruse, A. M. Ring, A. Manglik, J. Hu, K. Hu, K. Eitel, H. Hübner, E. Pardon, C. Valant, P. M. Sexton, A. Christopoulos, C. C. Felder, P. Gmeiner, J. Steyaert, W. I. Weis, K. C. Garcia, J. Wess, B. K. Kobilka, Activation and allosteric modulation of a muscarinic acetylcholine receptor. *Nature* **504**, 101–106 (2013).
57. W. Huang, A. Manglik, A. J. Venkatakrishnan, T. Laeremans, E. N. Feinberg, A. L. Sanborn, H. E. Kato, K. E. Livingston, T. S. Thorsen, R. C. Kling, S. Granier, P. Gmeiner, S. M. Husbands, J. R. Traynor, W. I. Weis, J. Steyaert, R. O. Dror, B. K. Kobilka, Structural insights into μ-opioid receptor activation. *Nature* **524**, 315–321 (2015).
58. W. Yin, Z. Li, M. Jin, Y.-L. Yin, P. W. de Waal, K. Pal, Y. Yin, X. Gao, Y. He, J. Gao, X. Wang, Y. Zhang, H. Zhou, K. Melcher, Y. Jiang, Y. Cong, X. E. Zhou, X. Yu, H. E. Xu, A complex structure of arrestin-2 bound to a G protein-coupled receptor. *Cell Res.* **29**, 971–983 (2019).
59. W. Huang, M. Masureel, Q. Qu, J. Janetzko, A. Inoue, H. E. Kato, M. J. Robertson, K. C. Nguyen, J. S. Glenn, G. Skiniotis, B. K. Kobilka, Structure of the neurotensin receptor 1 in complex with β-arrestin 1. *Nature* **579**, 303–308 (2020).
60. Y. Lee, T. Warne, R. Nehmé, S. Pandey, H. Dwivedi-Agnihotri, M. Chaturvedi, P. C. Edwards, J. García-Nafría, A. G. W. Leslie, A. K. Shukla, C. G. Tate, Molecular basis of β-arrestin coupling to formoterol-bound β_1-adrenoceptor. *Nature* **583**, 862–866 (2020).
61. D. P. Staus, H. Hu, M. J. Robertson, A. L. W. Kleinhenz, L. M. Wingler, W. D. Capel, N. R. Latorraca, R. J. Lefkowitz, G. Skiniotis, Structure of the M2 muscarinic receptor-β-arrestin complex in a lipid nanodisc. *Nature* **579**, 297–302 (2020).
62. X. Cong, D. Maurel, H. Déméné, I. Vasiliauskaité-Brooks, J. Hagelberger, F. Peysson, J. Saint-Paul, J. Golebiowski, S. Granier, R. Sounier, Molecular insights into the biased signaling mechanism of the μ-opioid receptor. *Mol. Cell* **81**, 4165–4175.e6 (2021).
63. R. Rahmeh, M. Damian, M. Cottet, H. Orcel, C. Mendre, T. Durroux, K. S. Sharma, G. Durand, B. Pucci, E. Trinquet, J. M. Zwier, X. Deupi, P. Bron, J.-L. Banères, B. Mouillac, S. Granier, Structural insights into biased G protein-coupled receptor signaling revealed by fluorescence spectroscopy. *Proc. Natl. Acad. Sci. U.S.A.* **109**, 6733–6738 (2012).
64. J. J. Liu, R. Horst, V. Katritch, R. C. Stevens, K. Wüthrich, Biased signaling pathways in β_2-adrenergic receptor characterized by ^{19}F-NMR. *Science* **335**, 1106–1110 (2012).
65. S. Bahrami, F. Drabløs, Gene regulation in the immediate-early response process. *Adv. Biol. Regul.* **62**, 37–49 (2016).
66. A. Kania, A. Gugula, A. Grabowiecka, C. de Ávila, T. Blasiak, Z. Rajfur, M. H. Lewandowski, G. Hess, E. Timofeeva, A. L. Gundlach, A. Blasiak, Inhibition of oxytocin and vasopressin neuron activity in rat hypothalamic paraventricular nucleus by relaxin-3-RXFP3 signalling. *J. Physiol.* **595**, 3425–3447 (2017).
67. W. T. Chance, S. Sheriff, T. Foley-Nelson, J. E. Fischer, A. Balasubramaniam, Pertussis toxin inhibits neuropeptide Y-induced feeding in rats. *Peptides* **10**, 1283–1286 (1989).
68. S. Sheriff, W. T. Chance, S. Iqbal, T. A. Rizvi, C. Xiao, J. W. Kasckow, A. Balasubramaniam, Hypothalamic administration of cAMP agonist/PKA activator inhibits both schedule feeding and NPY-induced feeding in rats. *Peptides* **24**, 245–254 (2003).
69. S. Sheriff, W. T. Chance, J. E. Fischer, A. Balasubramaniam, Neuropeptide Y treatment and food deprivation increase cyclic AMP response element-binding in rat hypothalamus. *Mol. Pharmacol.* **51**, 597–604 (1997).
70. G. C. Brailoiu, S. L. Dun, E. Brailoiu, S. Inan, J. Yang, J. K. Chang, N. J. Dun, Nesfatin-1: Distribution and interaction with a G protein-coupled receptor in the rat brain. *Endocrinology* **148**, 5088–5094 (2007).
71. C. L. Fitch, S. M. de Sousa, P. M. O'Day, T. A. Neubert, C. M. Plantilla, M. Spencer, S. Yarfitz, D. Apte, J. B. Hurley, Pertussis toxin expression in *Drosophila* alters the visual response and blocks eating behaviour. *Cell. Signal.* **5**, 187–207 (1993).
72. A. Inoue, F. Raimondi, F. M. N. Kadji, G. Singh, T. Kishi, A. Uwamizu, Y. Ono, Y. Shinjo, S. Ishida, N. Arang, K. Kawakami, J. S. Gutkind, J. Aoki, R. B. Russell, Illuminating G-protein-coupling selectivity of GPCRs. *Cell* **177**, 1933–1947.e25 (2019).
73. A. S. Dixon, M. K. Schwinn, M. P. Hall, K. Zimmerman, P. Otto, T. H. Lubben, B. L. Butler, B. F. Binkowski, T. Machleidt, T. A. Kirkland, M. G. Wood, C. T. Eggers, L. P. Encell, K. V. Wood, NanoLuc complementation reporter optimized for accurate measurement of protein interactions in cells. *ACS Chem. Biol.* **11**, 400–408 (2016).
74. K. Kawakami, M. Yanagawa, S. Hiratsuka, M. Yoshida, Y. Ono, M. Hiroshima, M. Ueda, J. Aoki, Y. Sako, A. Inoue, Heterotrimeric Gq proteins act as a switch for GRK5/6 selectivity underlying β-arrestin transducer bias. *Nat. Commun.* **13**, 487 (2022).
75. R. Ley, K. Balmanno, K. Hadfield, C. Weston, S. J. Cook, Activation of the ERK1/2 signaling pathway promotes phosphorylation and proteasome-dependent degradation of the BH3-only protein, Bim. *J. Biol. Chem.* **278**, 18811–18816 (2003).
76. J. H. Lee, P. R. Johnson, M. Roth, N. H. Hunt, J. L. Black, ERK activation and mitogenesis in human airway smooth muscle cells. *Am. J. Physiol. Lung Cell. Mol. Physiol.* **280**, L1019–L1029 (2001).
77. A. Braeuning, M. Menzel, E.-M. Kleinschnitz, N. Harada, Y. Tamai, C. Köhle, A. Buchmann, M. Schwarz, Serum components and activated Ha-ras antagonize expression of perivenous marker genes stimulated by β-catenin signaling in mouse hepatocytes. *FEBS J.* **274**, 4766–4777 (2007).
78. S. Liu, W. Yang, Y. Li, C. Sun, Fetal bovine serum, an important factor affecting the reproducibility of cell experiments. *Sci. Rep.* **13**, 1942 (2023).
79. B. Webb, A. Sali, Comparative protein structure modeling using MODELLER. *Curr. Protoc. Bioinformatics* **54**, 5.6.1–5.6.37 (2016).
80. D. L. Case, V. Babin, J. T. Berryman, R. M. Betz, Q. Cai, D. S. Cerutti, T. E. Cheatham, T. A. Darden, AMBER 14 (University of California, San Francisco, 2018).
81. J. A. Maier, C. Martinez, K. Kasavajhala, L. Wickstrom, K. E. Hauser, C. Simmerling, Ff14SB: Improving the accuracy of protein side chain and backbone parameters from ff99SB. *J. Chem. Theory Comput.* **11**, 3696–3713 (2015).
82. C. J. Dickson, B. D. Madej, A. A. Skjevik, R. M. Betz, K. Teigen, I. R. Gould, R. C. Walker, Lipid14: The AMBER lipid force field. *J. Chem. Theory Comput.* **10**, 865–879 (2014).
83. W. L. Jorgensen, J. Chandrasekhar, J. D. Madura, R. W. Impey, M. L. Klein, Comparison of simple potential functions for simulating liquid water. *J. Chem. Phys.* **79**, 926–935 (1983).
84. T. Darden, D. York, L. Pedersen, Particle mesh Ewald: An *N* log(*N*) method for Ewald sums in large systems. *J. Chem. Phys.* **98**, 10089–10092 (1993).
85. S. Miyamoto, P. A. Kollman, Settle: An analytical version of the SHAKE and RATTLE algorithm for rigid water models. *J. Comput. Chem.* **13**, 952–962 (1992).
86. W. Humphrey, A. Dalke, K. Schulten, VMD: Visual molecular dynamics. *J. Mol. Graph.* **14**, 33–38 (1996).
87. L. Schrodinger, The PyMOL Molecular Graphics System. 1.8 ed2015.
88. E. T. van der Westhuizen, B. Breton, A. Christopoulos, M. Bouvier, Quantification of ligand bias for clinically relevant β2-adrenergic receptor ligands: Implications for drug taxonomy. *Mol. Pharmacol.* **85**, 492–509 (2014).
89. B. A. Evans, M. Sato, M. Sarwar, D. S. Hutchinson, R. J. Summers, Ligand-directed signalling at β-adrenoceptors. *Br. J. Pharmacol.* **159**, 1022–1038 (2010).
90. T. Kenakin, C. Watson, V. Muniz-Medina, A. Christopoulos, S. Novick, A simple method for quantifying functional selectivity and agonist bias. *ACS Chem. Neurosci.* **3**, 193–203 (2012).
91. T. Kenakin, A. Christopoulos, Signalling bias in new drug discovery: Detection, quantification and therapeutic impact. *Nat. Rev. Drug Discov.* **12**, 205–216 (2013).

Acknowledgments: We thank W. F. Ho for excellent technical and administrative assistance. We thank A*STAR and NSCC, Singapore and the Faculty of Science, University of Colombo for support. We thank R. Bathgate (Florey Institute of Neuroscience and Mental Health, University of Melbourne) for providing HEK-RXFP3 cells. We thank L. Stanton (Genome Institute of Singapore) for the WT HEK293T cells. **Funding:** This work received support from the Ministry of Education, Singapore, Academic Research Fund Tier 1 funding programme (T1-NUHS O-CRG 2016 Oct-18 and T1-BSRG 2014-03) and Academic Research Fund Tier 3 funding programme (MOE2017-T3-1-002) (to G.S.D. and T.J.); Japan Science and Technology Agency (JST) JPMJPR1331, JPMJFR215T, and JPMJMS2023 (to A.I.); Japan Agency for Medical Research and Development (AMED) JP19gm5910013, JP19gm0010004, JP22ama121038, and JP22zf0127007 (to A.I.); Japan Society for the Promotion of Science (JSPS) JP21H04791, JP21H05113, and JP21H05037 (to A.I.); and A*STAR grant IAF-PP H1701a0010 (to C.S.V. and S.K.) **Author contributions:** Conceptualization: T.J. and G.S.D. Methodology: T.J., A.I., S.K., T.-B.N., and J.L. Investigation: T.J., A.I., S.K., G.N., K.K., T.-B.N., J.L., and D.R.H. Visualization: T.J., A.I., S.K., G.N., K.K., T.-B.N., J.L., and D.R.H. Supervision: G.S.D. and C.S.V. Writing—original draft: T.J., A.I., and S.K. Writing—review and editing: T.J., K.M., A.I., S.K., D.R.H., C.S.V., and G.S.D. **Competing interests:** S.K. and C.S.V. are founders of the biotech companies Sinopsee Therapeutics and Aplomex; however, this work presents no conflict. The other authors declare that they have no competing interests. **Data and materials availability:** All data needed to evaluate the conclusions in the paper are present in the paper or the Supplementary Materials. The NanoBiT constructs are available through a material transfer agreement from Tohoku University.

Submitted 22 July 2021
Resubmitted 9 January 2023
Accepted 26 January 2024
Published 13 February 2024
10.1126/scisignal.abl5880